

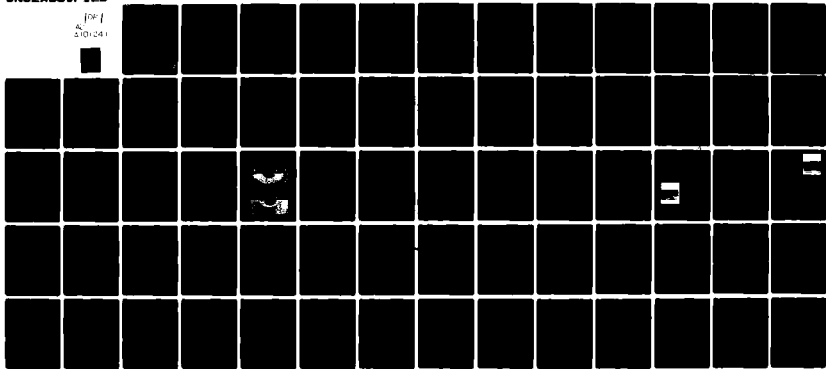
AD-A101 241

STANFORD UNIV CA EDWARD L GINZTON LAB OF PHYSICS F/G 11/2  
SURFACE ACOUSTIC WAVE MEASUREMENTS OF SURFACE CRACKS IN CERAMIC--ETC(U)  
JUN 81 J J TIEN, B T KHURI-YAKUB, B S KING N00014-78-C-0263

UNCLASSIFIED

NL

for  
2004



END  
DATE  
FILMED  
8-81  
DTIC

AD A101241

SURFACE ACOUSTIC WAVE MEASUREMENTS OF SURFACE CRACKS IN CERAMICS,

J.J.W./Tien, B.T./Khuri-Yakub, G.S./Kino  
Edward L. Ginzton Laboratory  
Stanford University  
Stanford, California 94305

and

D.B. Marshall, A.G. Evans  
Department of Materials Science and Mineral Engineering  
University of California  
Berkeley, California 94720

June 1981

Abstract

An investigation of scattering from surface cracks has been conducted. In particular, the change in the reflection coefficient of a Rayleigh wave incident on a surface indentation crack has been measured as the sample is stressed to fracture. The acoustic measurements have been correlated with the stable crack extension that precedes final failure. The crack extension behavior in as-indented and annealed specimens was found to be appreciably different. The cracks in the annealed samples exhibited partial crack closure but little stable extension, whereas the cracks in the as-indented samples displayed both crack closure and irreversible crack growth. This behavior has been rationalized by invoking concepts based upon the residual stresses created by indentation.

DTIC FILE COPY

This document has been approved for public release and sale; its distribution is unlimited.

DTIC ELECTE

JUL 2 1981

81 6 12 080

A

JE

## I. INTRODUCTION

The use of surface acoustic waves to detect and characterize surface cracks in brittle materials has been described in previous studies.<sup>1,2</sup> The basic technique devised in these studies requires the excitation of a Rayleigh wave on the surface of the brittle solid and the subsequent observation of the acoustic wave reflections from the surface located cracks. The first studies<sup>1</sup> were performed on glass samples containing surface cracks introduced by indentation and then extended to a larger size by application of a sub-critical stress. The acoustic measurements were conducted with a small stress applied to the specimen in order to eliminate crack closure. These studies indicated that acoustic measurements performed in the long wavelength regime provided precise predictions of the failure strength of the glass specimens. Subsequent studies were conducted on  $\text{Si}_3\text{N}_4$  specimens.<sup>2</sup> The surface cracks subject to acoustic measurements in these studies were created by direct indentation without introducing an intermediate extension procedure. The final fracture stresses obtained in the test specimens could be adequately predicted from the acoustic measurements, but only by invoking an effective fracture toughness smaller than the actual toughness of the material by ~30% (see Appendix). Additionally, the acoustic estimates of the crack radius were invariably smaller than the subsequently measured crack radii (at the fracture criticality) by a factor of ~2.5. Cracks of this type are typical of machining-induced cracks,<sup>3</sup> and hence, an adequate comprehension of such discrepancies is needed before applying surface acoustic wave techniques to the prediction of failure of components subject to surface finishing by machining.

Recent studies of indentation fracture<sup>4-7</sup> have demonstrated that the cracking behavior is dominated by the residual field created during the indentation process. This residual field causes indentation cracks to extend when an external stress is applied.<sup>6</sup> The initial extension is stable; instability commences when the crack attains a length ~2.5 times the initial length. This residual stress effect is almost certainly the origin of the discrepant acoustic predictions. The phenomenon is examined in the present study by monitoring the acoustic scattering from a surface crack as an external stress is applied to the test specimen.

The residual stress can be essentially eliminated by annealing at temperatures (~1200°C for Si<sub>3</sub>N<sub>4</sub>) at which dislocation climb and annihilation can proceed. Correctly annealed specimens should thus exhibit no stable crack extension and an enhanced fracture strength. Hence, the influence of annealing on both the acoustic scattering and the failure prediction is also examined.

Finally, implications for predicting the failure of machined components from surface acoustic wave measurements are discussed. Emphasis is placed upon the choice of an optimum measurement procedure and the role of annealing.

## II. ACOUSTIC SCATTERING FROM SURFACE CRACKS

A general theory of scattering from flaws<sup>8,9</sup> forms the basis for the present study. The scattering configuration is shown in Fig. 1. The quantity of interest is the relative amplitude of the acoustic signal scattered by the flaw. This quantity is given by the reflection coefficient  $S_{21}$  and is defined as the ratio of the amplitude of the signal reflected from the flaw,

$A_2$  (received by transducer 2) to the amplitude of the incident signal,  $A_1$  (transmitted by transducer 1), at the terminals of the transducers. Expressed in terms of the input power to the transmitting transducer,  $P_R$ , the Rayleigh wave displacement field (when the receiving transducer is used as the transmitter)  $u_j^{(2)}$ , and the prior stress in the vicinity of the flaw,  $\sigma_{ij}^{A(1)}$ , the reflection coefficient for a void is given by

$$S_{21} \equiv \frac{A_2}{A_1} = \frac{j\omega}{4P_R} \int_{S_c} u_j^{(2)} \sigma_{ij}^{A(1)} n_i dS \quad (1)$$

Here, the integral is taken over the entire surface of the void,  $S_c$ . For a Rayleigh wave normally incident on a half-penny shaped surface crack of radius  $a$  located in the  $x$ - $y$  plane (Fig. 2), Eq. (1) becomes

$$S_{11} = \frac{j\omega}{4P_R} \int_S \Delta u_z \sigma_{zz}^A dS \quad (2)$$

where  $\Delta u_z$  is the discontinuity in displacement across the crack and  $\sigma_{zz}^A$  is the prior normal stress. The integral is taken over just the semi-circular area,  $S$ . The theory is strictly valid only in the low frequency regime (i.e. where the maximum depth to which the crack extends below the sample surface is required to be much less than an acoustic wavelength). The scattering from surface cracks is also influenced by imaging at the surface (which increases the value of the stress intensity factor) and the variation with depth of the Rayleigh wave stress field. These influences are incorporated into the analysis by adopting the results of Budiansky and O'Connell<sup>10</sup> which permit the surface integral in Eq. (2) to be expressed in

terms of a contour integral

$$\int_S \Delta u_z \sigma_{zz}^A dS = \frac{2(1 - \nu^2)}{3E} \int_C \rho(\vec{r}) K_I^2(\theta) d\ell \quad (3)$$

where  $\nu$  is Poisson's ratio,  $E$  is Young's modulus,  $K_I$  is the mode I stress intensity factor, and  $\rho(\vec{r})$  is defined for a given point  $\vec{r}$  on the crack circumference  $C$  as the normal to the tangent line at  $\vec{r}$  which also passes through the origin of the crack coordinate system. The angular dependence of  $K_I$  caused by the surface imaging forces may be approximated from the results of Smith, Emery, and Kobayashi<sup>11</sup> for a half-penny shaped surface crack in a beam of thickness  $2c$  subject to a bending load. The applied stress then takes the linear form

$$\sigma_{zz}^A(y) = \beta(1 - y/c) \quad (4)$$

where  $\beta$  is a constant and  $y$  is the distance from the sample surface (Fig. 2). The corresponding stress intensity factor is given by

$$K_I(\theta) = 2\sqrt{a/\pi} \beta [\psi_0(\theta) - (a/c) \psi_1(\theta)] \quad (5)$$

where the functions  $\psi_0(\theta)$  and  $\psi_1(\theta)$  have been numerically evaluated (Fig. 3). These solutions are used to provide an approximate surface wave scattering result by adopting a linear approximation to the Rayleigh wave stress field and deducing effective values for the constants  $\beta$  and  $c$ . The normalized reflection coefficient  $wk|S_{11}|$  for a semi-circular crack obtained

in this manner is plotted as a function of the normalized crack depth,  $2\pi a/\lambda$ , in Fig. 4. Here  $k = 2\pi/\lambda$  is the propagation constant of the Rayleigh wave, and  $w$  is the width of the acoustic beam at the location of the crack.

### III. EXPERIMENTAL RESULTS

A commercial hot-pressed silicon nitride (NC-132) was used for the present study. The samples were in the form of 7.6 cm x 2.6 cm x 0.64 cm plates with polished surfaces. A crack was introduced into the center of each plate surface (normal to the longer edge) by Knoop indentation at 50N load. Acoustic measurements were made at a frequency of 8.5 MHz, corresponding to an acoustic wavelength of  $\sim 680 \mu\text{m}$ . Two wedge transducers in the configuration shown in Fig. 1 (with  $\alpha = 12.5^\circ$ ) were used to excite and receive the acoustic signals. The experimental values for the reflection coefficient were corrected for diffraction loss, the surface wave conversion efficiencies of the transducers, and for the inclination of the transmitted and reflected acoustic beams to the crack normal.

Measurements were performed on both annealed and as-indented samples. One sample was annealed in air and another in a vacuum for an annealing period of about six hours at a temperature of  $1200^\circ\text{C}$ . An additional three samples were tested in the as-indented state. In all cases, the change in the acoustic reflection coefficient was monitored while the samples were slowly stressed to fracture in a flexural mode. Typical variations of the reflection coefficient (expressed in terms of a predicted crack radius - see Section IV) with the magnitude of the applied flexural stress are plotted in Fig. 5.

Substantially different behavior is apparent in the as-indentured and annealed specimens. The as-indentured samples exhibit a large change in the reflection coefficient as the flexural stress is slowly increased to failure. Also, the change is largely irreversible, as manifest in a permanent increase in  $S_{11}$  following the load removal prior to failure (Fig. 5a). This behavior suggests stable crack extension during the application of an external stress, qualitatively consistent with the residual stress notions of indentation fracture.<sup>6</sup> The existence of stable crack extension was substantiated by observations of the fracture initiation site on the fracture surface (Fig. 6a). These observations indicate an inner crack front location that coincides with the initial radius  $a_0$  of the indentation crack and an outer crack front with a radius  $a_c \approx 2.5a_0$ . The outer front is presumed to be the location of the crack at the fracture criticality, as suggested by observations on other materials.<sup>3,5</sup>

The annealed specimens (Fig. 5b) exhibited appreciably larger final levels of the fracture stress (the elevation of the fracture stress is similar to that measured in prior studies).<sup>12</sup> The vacuum-annealed specimen exhibited small reversible changes in the acoustic scattering during stressing, a phenomenon that will be attributed to the gradual, reversible separation of the crack surfaces (see Section IV.B). Observations of the fracture origin (Fig. 6b) revealed closely spaced crack fronts, indicating that stable crack extension had been largely eliminated by the annealing treatment. Some stable extension may have occurred just prior to instability in the range of rapidly varying crack length indicated in Fig. 6b.

The specimen annealed in air (Fig. 5c) exhibited an additional increment in the scattering coefficient at about one third of the fracture stress. This effect may be attributed to the fracture of the oxide film that forms within the crack when annealing is conducted in an oxidizing environment.

#### IV. DISCUSSION

##### A. As-Indented Specimens

The acoustic scattering and the fracture response exhibited by as-indented specimens are both influenced by specific characteristics of the indentation plasticity and the indentation morphology. The important relationship between scattering, fracture, and indentation can be established by invoking the appropriate indentation parameters. The acoustic scattering from an indentation crack can be interpreted by noting that the residual stress field (attributed to the elastic constraint of the indentation plasticity)<sup>7</sup> allows the crack surfaces in the elastic region to remain fully separated when the indentation load is removed. However, the crack terminates in the vicinity of the elastic/plastic boundary (Fig. 7a). The crack thus exhibits the morphology of a semi-annulus, with the inner radius dictated by the radius of the plastic zone. This crack geometry is not amenable to acoustic scattering analysis using conventional analytic techniques. An approximate solution is thus developed for preliminary crack size estimation. The solution considers the open region of the crack to be elliptical in section, with the major axis,  $2a$ , given by the crack diameter and the minor axis,  $2b$ , given by the difference between the crack depth and the plastic zone depth (Fig. 7b). In essence, therefore, the crack is

considered to be held fully closed at the specimen surface by virtue of the integrity of the plastic zone. The scattering induced by an elliptical crack subject to a linearly varying stress (the linearized Rayleigh wave stress field) should thus provide the approximate solution of present interest. The stress intensity factor that characterizes this configuration is given by<sup>13</sup>

$$K_I(\theta) = \frac{\sqrt{\pi b/a}}{E(k)} (a^2 \cos^2 \theta + b^2 \sin^2 \theta)^{1/4} C_1 M_T(\theta) + C_2 M_L(\theta) \left[ 1 - \frac{k^2 E(k) \cos \theta}{(1 + k^2) E(k) - (k')^2 K(k)} \right] \quad (6)$$

where  $K(k)$  and  $E(k)$  are complete elliptical integrals of the first and second kinds, respectively, with  $k^2 = 1 - (b/a)^2$  and  $(k')^2 = (b/a)^2$ .

$M_T(\theta)$  and  $M_L(\theta)$  represent the stress intensity magnification factors (Fig. 8) for an elliptical crack subject, respectively, to a uniform applied stress and a linearly varying applied stress, and  $C_1$  and  $C_2$  are constants that characterize the linearized Rayleigh wave stress

$$\sigma_{zz}^A(y) = C_1 + C_2 \frac{b - y}{b} \quad (7)$$

The stress intensity factor can be inserted into Eqs. (2) and (3) in order to compute the scattering coefficient. The result for the normalized reflection coefficient,  $wk|S_{11}|$ , as a function of the normalized crack depth,  $2\pi(b + h)/\lambda$ , is given by the solid curve in Fig. 4. A comparison of the acoustic estimates for the initial crack depth,  $C_0$ , and the depth at fracture,  $C_m$ , with the corresponding values measured optically is given in

Table I. From the acoustic estimates for the initial crack depth, a prediction for the fracture stress of each sample may further be made by using the relation

$$\sigma_F^{\text{Acoustic}} = \frac{K_{IC}}{k_I|_{\text{surf}}} \quad (8)$$

where

$$k_I|_{\text{surf}} = 1.22 k_I|_{\text{bulk}} = 1.22(2\sqrt{a/\pi}) \quad (9)$$

and  $K_{IC} = 3.55 \text{ MPa}\sqrt{\text{m}}$ .<sup>14</sup> These predictions for the fracture stresses are compared with the actual fracture stress values in Table II. Considering the approximate nature of the scattering analysis, both comparisons yield remarkably good agreement.

The fracture process is strongly influenced by the magnitude of the residual stress induced by the plastic zone. The extension of an indentation crack under the combined influence of an external stress and the residual indentation stress has been predicted for axisymmetric indentations by invoking residual stress concepts.<sup>6</sup> The direct applicability of these predictions to elongated indentations, such as Knoop indentation, has not yet been verified in detail. However, it is instructive to compare the axisymmetric predictions with the acoustic measurements of crack extension. The following expression relates the equilibrium crack radius,  $a$ , to the external stress  $\sigma_\infty$ .

$$\sigma_{\infty} = \frac{K_{IC}}{(\pi\Omega a)^{1/2}} \left[ 1 - \frac{x_r^P}{K_{IC} a^{3/2}} \right] \quad (10)$$

where  $K_{IC}$  is the material's fracture toughness,  $P$  is the indentation load,  $x_r$  is a parameter (related to material hardness and elastic modulus) which determines the intensity of the residual field, and  $\Omega$  is a material independent crack geometry constant. According to Eq. (10), the crack length increases stably with applied stress from the initial value (given by Eq. (10) with  $\sigma_{\infty} = 0$ )

$$a_0 = (x_r^P / K_{IC})^{2/3} \quad (11)$$

to the failure point (given by  $d\sigma_{\infty}/da = 0$  in Eq. (10))

$$a_m = (4x_r^P / K_{IC})^{2/3} \quad (12)$$

$$\sigma_m = (27/256)^{1/3} [K_{IC}/(\pi\Omega)^{1/2}] [K_{IC}/x_r^P]^{1/3} \quad (13)$$

The parameters  $K_{IC}(\pi\Omega)^{1/2}$  and  $x_r^P/K_{IC}$  required for plotting Eq. (10) can be conveniently calibrated from the calculated (from acoustic measurements) initial crack length and the measured fracture stress. Setting  $a_0 = 96 \mu\text{m}$  in Eq. (11) gives  $x_r^P/K_{IC} = 9.2 \times 10^{-7} \text{m}^{3/2}$ , while the measured strength  $\sigma_m = 240 \text{ MPa}$  in conjunction with Eq. (13) gives  $K_{IC}/\sqrt{\pi\Omega} = 4.95 \text{ MPa}\sqrt{\text{m}}$ . The predicted dependence of crack extension on applied stress is shown in Fig. 5a. The prediction correlates well with the acoustic measurements of changes in crack length.

## B. Annealed Specimens

Removal of residual stress by annealing results in the development of crack surface contacts over an appreciable fraction of the surface (Fig. 9). Complete closure over the contacting region is prevented by "asperities" along the crack surface. The asperities comprise either grains dislodged by crack bifurcation or exposed grains in which residual stress (due to thermal contraction anisotropy) has been relaxed by the passage of the crack, thus causing the grains to displace. Compressive forces must develop at the contact locations due to elasticity of the surrounding material.<sup>15</sup> The forces are maximum close to the crack tip and decrease to zero at some distance  $a_i$  (Fig. 9). The area subject to zero contact forces defines a non-contacting crack radius  $a_i$ . The compressive forces allow the contacts to be retained in the presence of an acoustic stress. Hence the scattering from the contacting region of the crack surface is negligible\* and the acoustic scattering amplitude only provides a measure of the non-contacting crack radius (Fig. 9).

The compressive tractions at the asperities are relaxed by application of an external tensile stress. An analysis of the crack separation process<sup>15</sup> indicates that separation initiates from the periphery of the initial non-contacting zone and extends as the external stress increases. Full crack

\*Scattering occurs from the regions between the asperities within the contact area. However, since these scattering centers act as small cracks (with radii approximately equal to several grain diameters) and the scattering amplitude is (to lowest order) proportional to  $a^3$ , the total scattered amplitude from the contacting area is small compared with that from the non-contacting area.

surface separation occurs immediately prior to unstable crack extension. The crack separation process is reversible, and this process fully accounts for the changes in acoustic crack length that occur during a breaking test.

#### V. IMPLICATIONS AND CONCLUSIONS

A combined acoustic, fracture mechanics study has demonstrated that long wavelength, surface acoustic wave scattering measurements can provide good estimates of the dimensions of surface located cracks and that the crack dimensions can be clearly related to the ultimate failure strength. The connection between the failure condition and the initial crack size estimate depends upon the state of residual crack stress induced by the machining (or indentation) process. The most severe residual stress exists immediately following the machining increment that generated the crack subject to acoustic investigation. Subsequent machining passes will remove portions of the plastic zone and successively reduce the residual stress. However, the state of residual stress at a specific machining-induced crack, identified by acoustic inspection, will generally be unknown. A failure prediction procedure that recognizes the most detrimental residual stress condition is thus recommended.

The most consistent acoustic crack size estimation can be conducted in the presence of the residual stress because the crack surfaces are fully separated. Therefore the acoustic measurements should be conducted on the as-machined surface. The failure strength prediction should be based upon the crack size estimation procedure pertinent to indentation cracks, using the effective value of the initial stress intensity factor (Appendix) that fully

accounts for the (residual stress-induced) stable extension prior to failure. This procedure will provide a conservative prediction of failure for many of the cracks detected on a machined surface because some of the residual stress will have been relaxed by partial plastic zone removal. However, the unknown state of the residual stress necessitates the conservative choice. Finally, it is recommended that the components be annealed prior to use in order to relieve the remnant residual stresses. The stress relief will provide an appreciable margin of safety for most cracks.

At this juncture, it is not considered appropriate to anneal the component prior to acoustic evaluation because the variability in the crack closure is likely to provide imprecise estimates of the actual crack length. However, further investigation of crack closure effects may suggest effective procedures for generating consistent acoustic measurements. Finally, it is noted that the strength of annealed specimens deduced from acoustic measurements on machined surfaces may be a consistent underestimate, whereupon the failure strength prediction could be elevated above the minimum level presently recommended. The origin of such an underestimate would reside in the relative influences of crack closure and of the residual stress level on the relation between the acoustic scattering amplitude and the residual strength. Again, studies of crack closure effects will permit such possibilities to be fully exploited.

Acknowledgment

This work was supported by the Office of Naval Research under Contract  
N00014-78-C-0283.

APPENDIX

Relation Between Failure Strength  
and Initial Size of Indentation Cracks

Previous studies have demonstrated that in order to relate the final fracture stress of indentation flaws to the initial flaw size using the Griffith strength equation, an effective toughness smaller than the actual material toughness must be invoked. This result can also be derived from a fracture mechanics analysis which takes into account the influence of residual stresses induced by the plastic indentation zone. For axisymmetric indentations the fracture stress can be written (using Eqs. (11) and (13))

$$\sigma_m = \frac{27}{256} \frac{K_{IC}^{1/3}}{(\pi \Omega a_0)^{1/2}} \quad (A-1)$$

Hence, in the idealized case, the effective toughness is  $K_{eff} = 0.47 K_{IC}$ . In practice, several factors can increase  $K_{eff}$  above the idealized value. Firstly, the incidence of lateral cracking, or chipping, after the formation of the median crack diminishes the residual field, as characterized by the parameter  $\chi_r$  in Eq. (13). This effect can cause  $K_{eff}$  to exceed the idealized value. Secondly, in materials susceptible to subcritical crack growth, the initial flaw size can increase under the influence of the residual stress, during the time period between the indentation and strength tests. Again, the consequence is an increase in  $K_{eff}$ . Finally, the influence of the elongated geometry of the Knoop indentation may alter the numerical constant in Eq. (A-1). Typically, for Knoop indentation pre-cracks in  $Si_3N_4$ ,

$$K_{eff} \approx 2/3 K_{IC}^{.12}$$

TABLE I: As-Indented Samples

$C_0$  = initial crack depth  
 $C_m$  = crack depth at fracture

Sample	Acoustic $C_0$ ( $\mu\text{m}$ )	Actual $C_0$ ( $\mu\text{m}$ )	Deviation ( $C_0$ )	Acoustic $C_m$ ( $\mu\text{m}$ )	Actual $C_m$ ( $\mu\text{m}$ )	Deviation ( $C_m$ )
4	97	116	16%	184	220	16%
5	94	112	16%	191	223	14%
6	96	112	14%	185-191	205	7-10%

TABLE II: Fracture Stresses (As-Indented Samples)

Sample	Acoustic $\sigma_F$ (MPa)	Actual $\sigma_F$ (MPa)	Deviation
4	262	238	10%
5	266	239	11%
6	263	242	9%

#### REFERENCES

1. B.T. Khuri-Yakub, A.G. Evans, and G.S. Kino, J. Am. Ceramic Soc. 63 65 (1980).
2. J. Tien, B. Khuri-Yakub, and G.S. Kino, Proc. ARPA/AFML Rev. of Progress in Quantitative NDE, La Jolla, California, (1979).
3. D.B. Marshall, B.R. Lawn, and J. Mecholsky, J. Am. Ceramic Soc. 63 358-360 (1980).
4. D.B. Marshall, B.R. Lawn, and P. Chantikul, J. Mat. Science 14 2001-2012 (1979).
5. D.B. Marshall, B.R. Lawn, and P. Chantikul, J. Mat. Science 14 2225-2235 (1979).
6. B.R. Lawn and D.B. Marshall, J. Am. Ceramic Soc. 62 106-108 (1979).
7. B.R. Lawn, A.G. Evans, and D.B. Marshall, J. Am. Ceramic Soc. 63 574-581 (1980).
8. G.S. Kino, J. Appl. Phys. 49 3190-3199 (1978).
9. B.A. Auld, Wave Motion 1 3-10 (1979).
10. B. Budiansky and R.J. O'Connell, Int. J. Solid Struc. 12 81-97 (1976).
11. F.W. Smith, A.F. Emery, and A.S. Kobayashi, J. Appl. Mech. 34 953-959 (1967).
12. J.J. Petrovic, R.A. Dirks, L.A. Jacobson, and M.G. Mendiratta, J. Am. Ceramic Soc. 59 177-178 (1976).
13. R.C. Shah and A.S. Kobayashi, "On the Surface Flaw Problem," in The Surface Crack: Physical Problems and Computational Solutions, J.L. Swedlow, ed. 79-124 (1972).

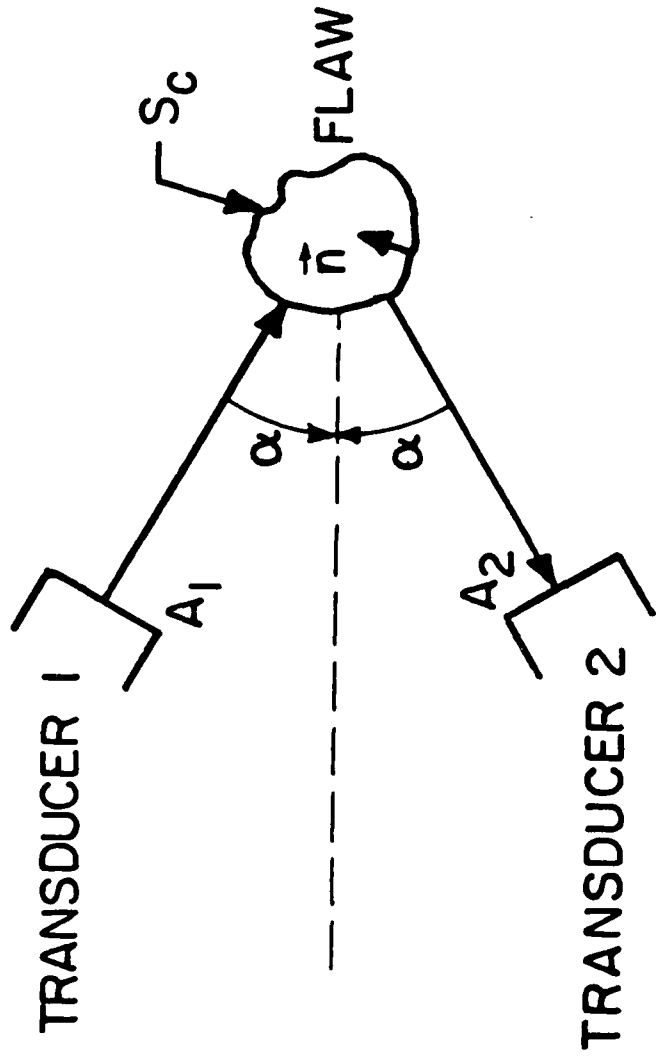
14. J.J. Petrovic, I.A. Jacobson, P.K. Talty, and A.K. Vasudevan, J. Am. Ceramic Soc. 58 113-116 (1975).
15. A.G. Evans, B. Budiansky, and G.S. Kino, unpublished.

#### FIGURE CAPTIONS

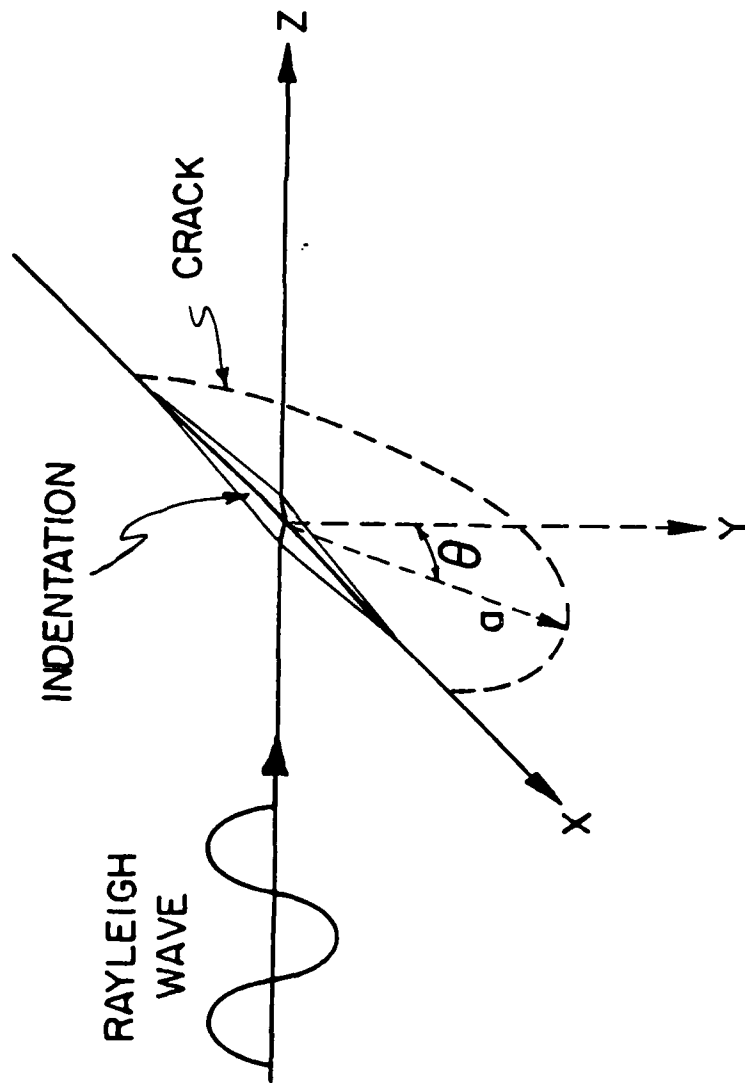
1. A schematic of the geometry considered in the derivation of the reflection coefficient,  $S_{21}$ , for a flaw. Here,  $\vec{n}$  is the inward normal to the flaw surface,  $S_c$ , and  $\alpha$  is the inclination of the flaw to the transducers.
2. Scattering geometry for a Rayleigh wave normally incident on a half-penny shaped crack.
3. Angular variation of the functions  $\psi_0(\theta)$  and  $\psi_1(\theta)$  (after Smith et al.).<sup>11</sup>
4. Comparison of the results for the normalized reflection coefficient,  $wk|S_{11}|$ , as a function of the normalized crack depth for the half-penny shaped crack theory and the elliptical crack theory. The normalized crack depth is defined for each theory by the quantities  $2\pi a/\lambda$  and  $2\pi(b+h)/\lambda$ , respectively.
5. The variation of the crack depth (obtained from the acoustic scattering amplitude) with the flexural stress.
  - (a) As-indented specimen: note the irreversibility of the crack length indicated by the permanent change following unloading. Also shown is the crack change predicted from the indentation model;
  - (b) Vacuum-annealed specimen indicating irreversibility;
  - (c) Oxygen-annealed specimen.
6. Optical micrographs of fracture origins:
  - (a) As-indented specimens indicating an initial crack front much smaller than the crack front at instability;

(b) Vacuum-annealed specimens showing a small zone of stable crack extension.

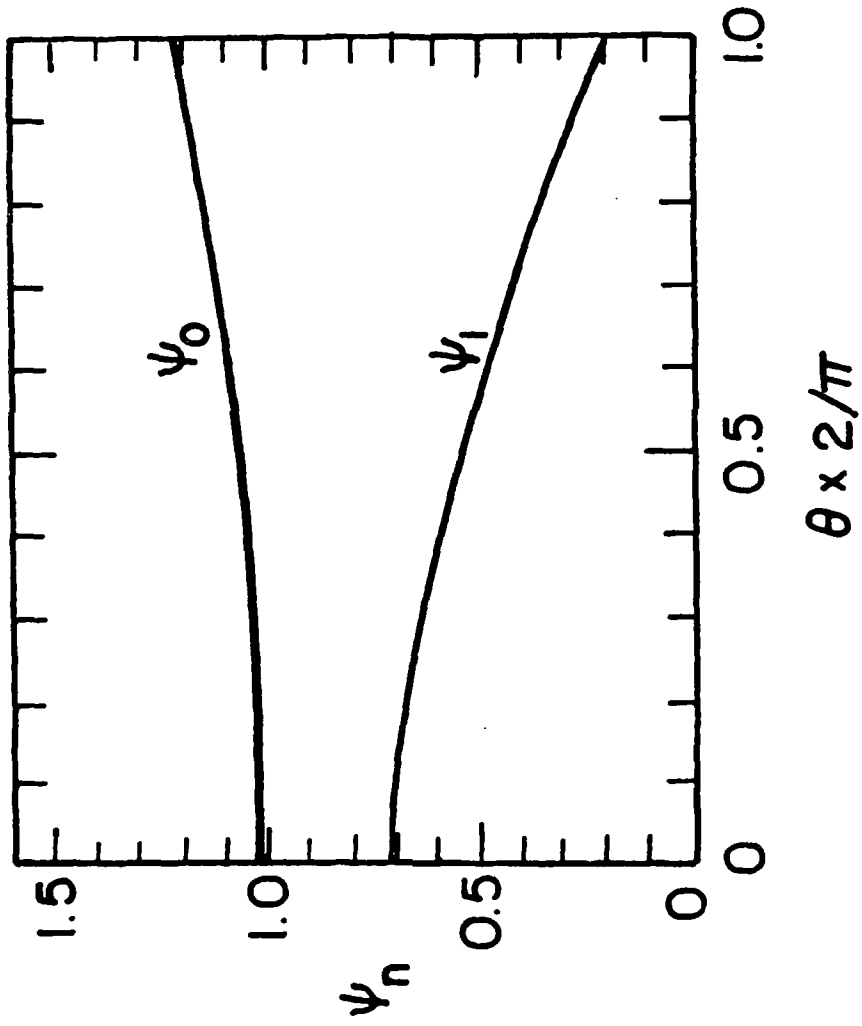
7. (a) A schematic of an as-indentated crack indicating that crack closure is exhibited over the plastic zone;  
(b) A subsurface elliptical crack analog of (a) used for acoustic scattering analysis.
8. Stress intensity magnification factors  $M_T(\theta)$  and  $M_L(\theta)$  as functions of the angle  $\theta$  for the elliptical crack configuraion of Fig. 8b, subject to a uniform applied stress and a linearly varying applied stress, respectively.
9. The crack configuration in annealed specimens indicating the zone of contact and the compressive forces that exist at asperities in the region.



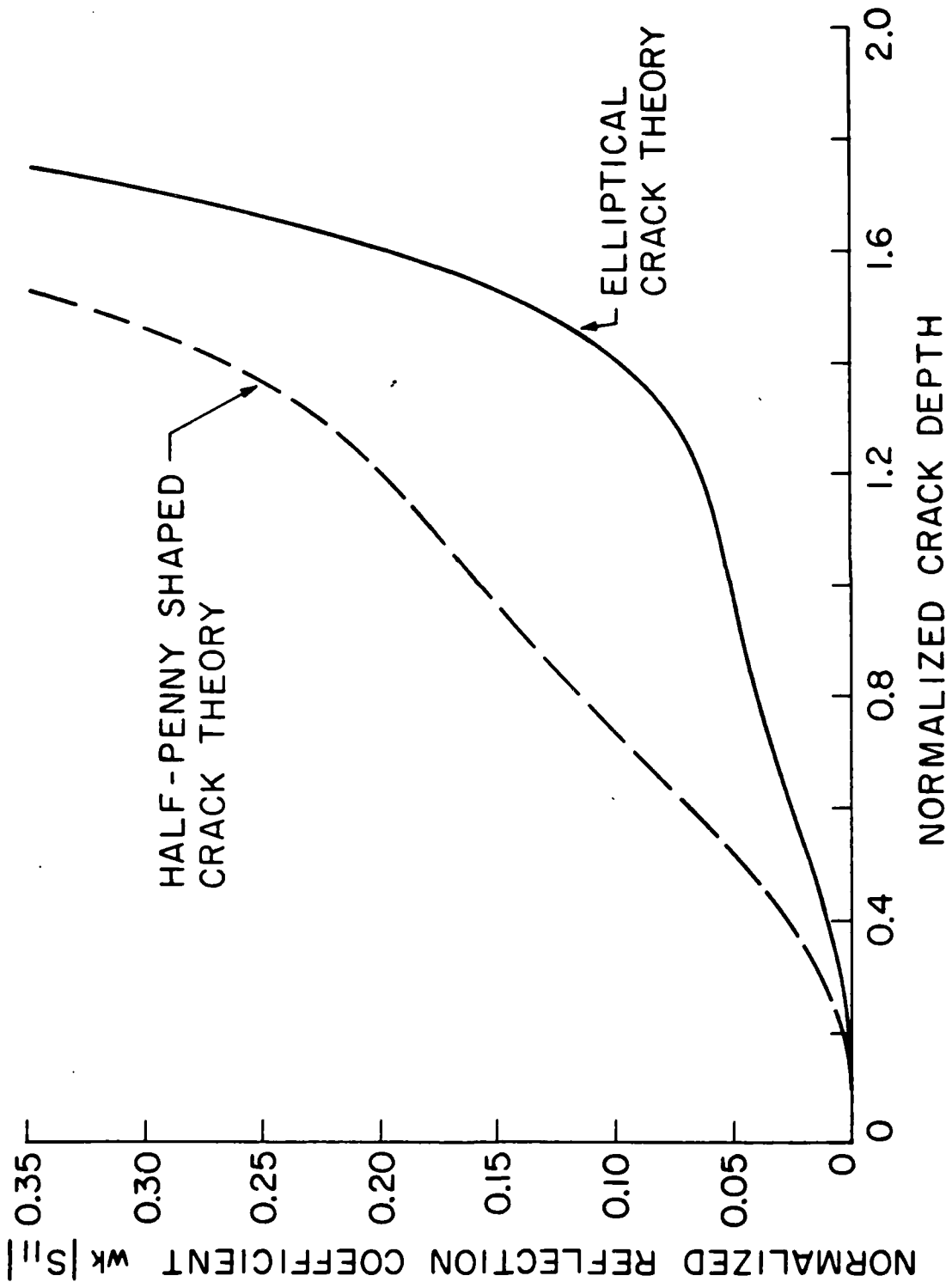
XBL8012-13372

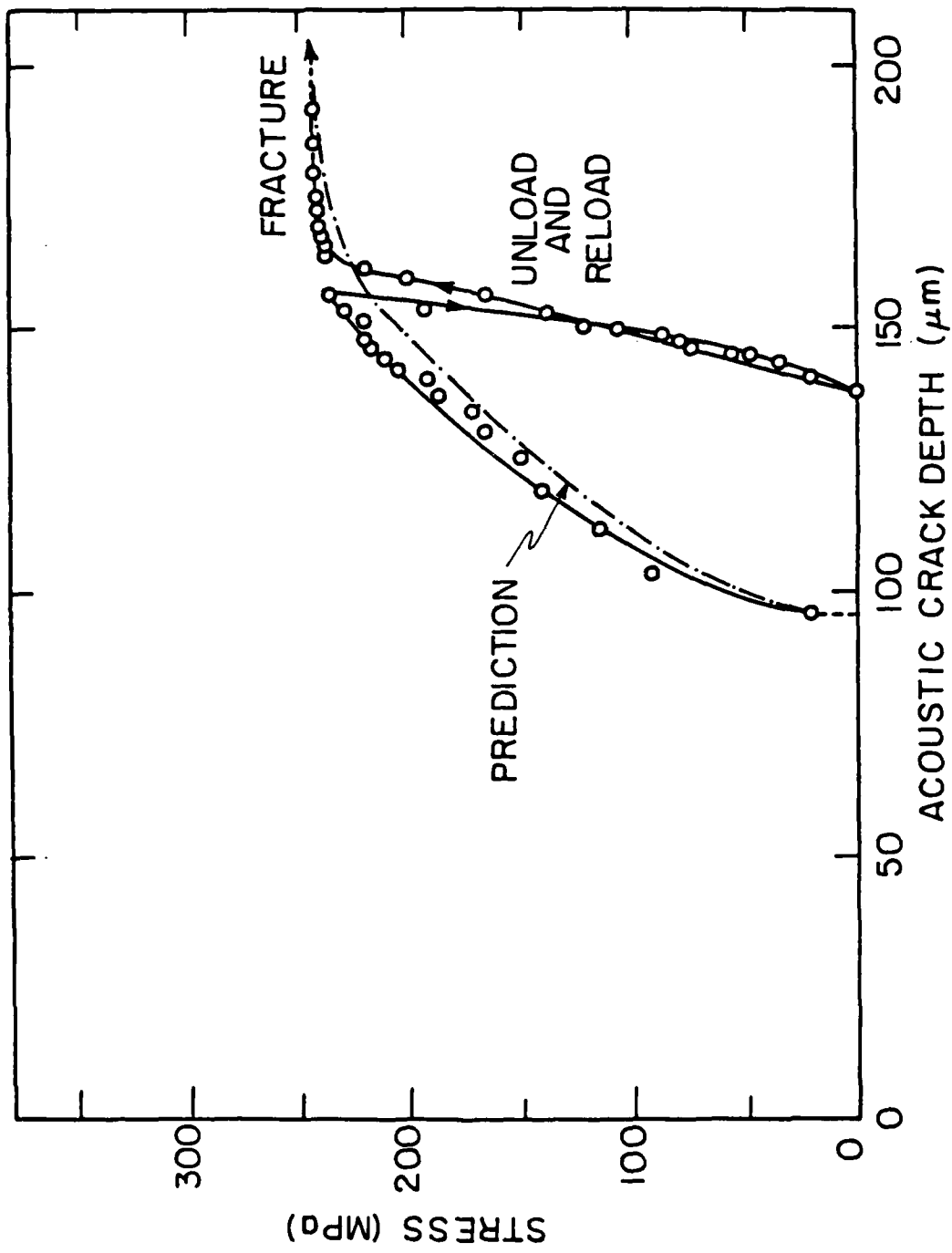


XBL 8012-13373

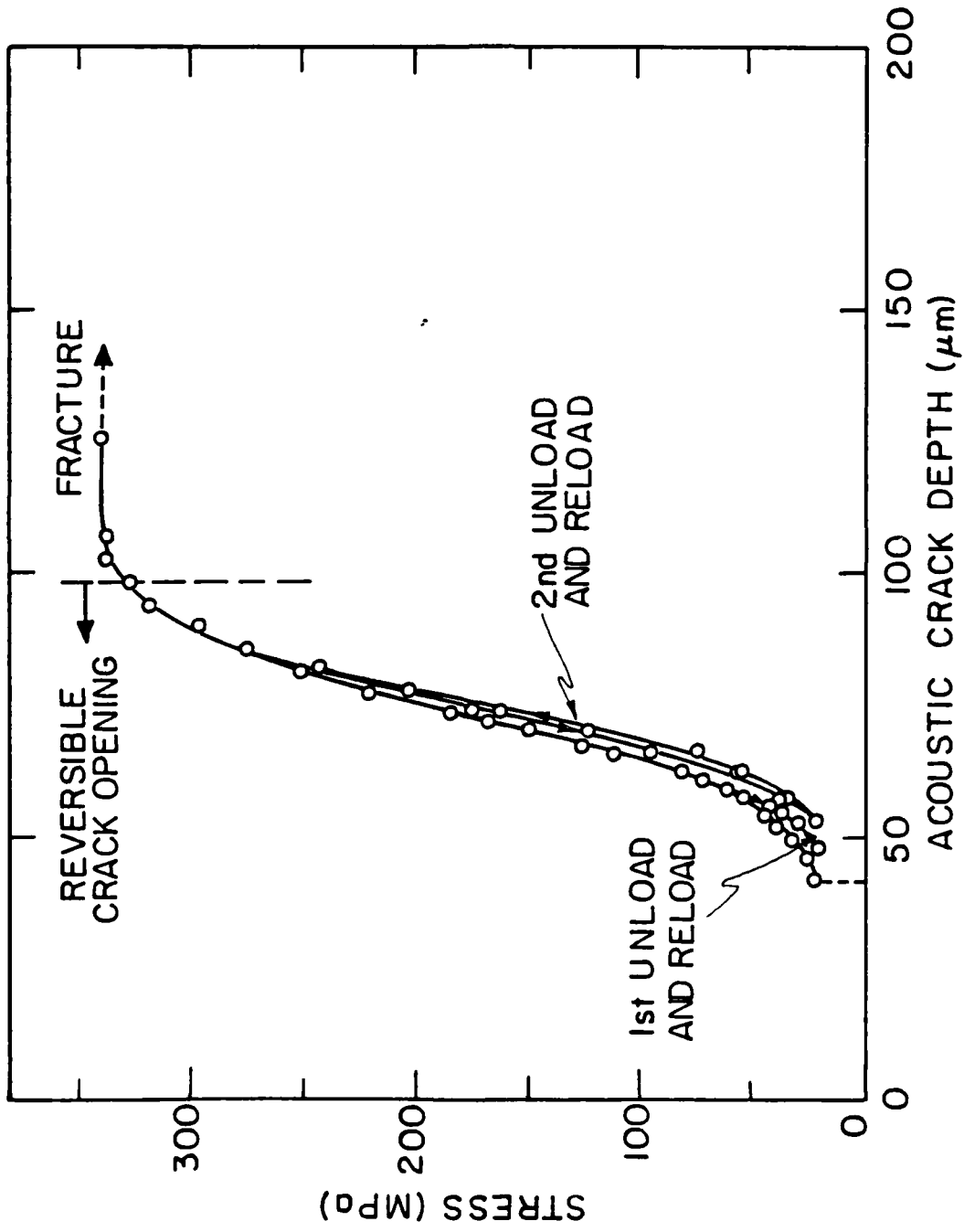


XBL 8012-13374

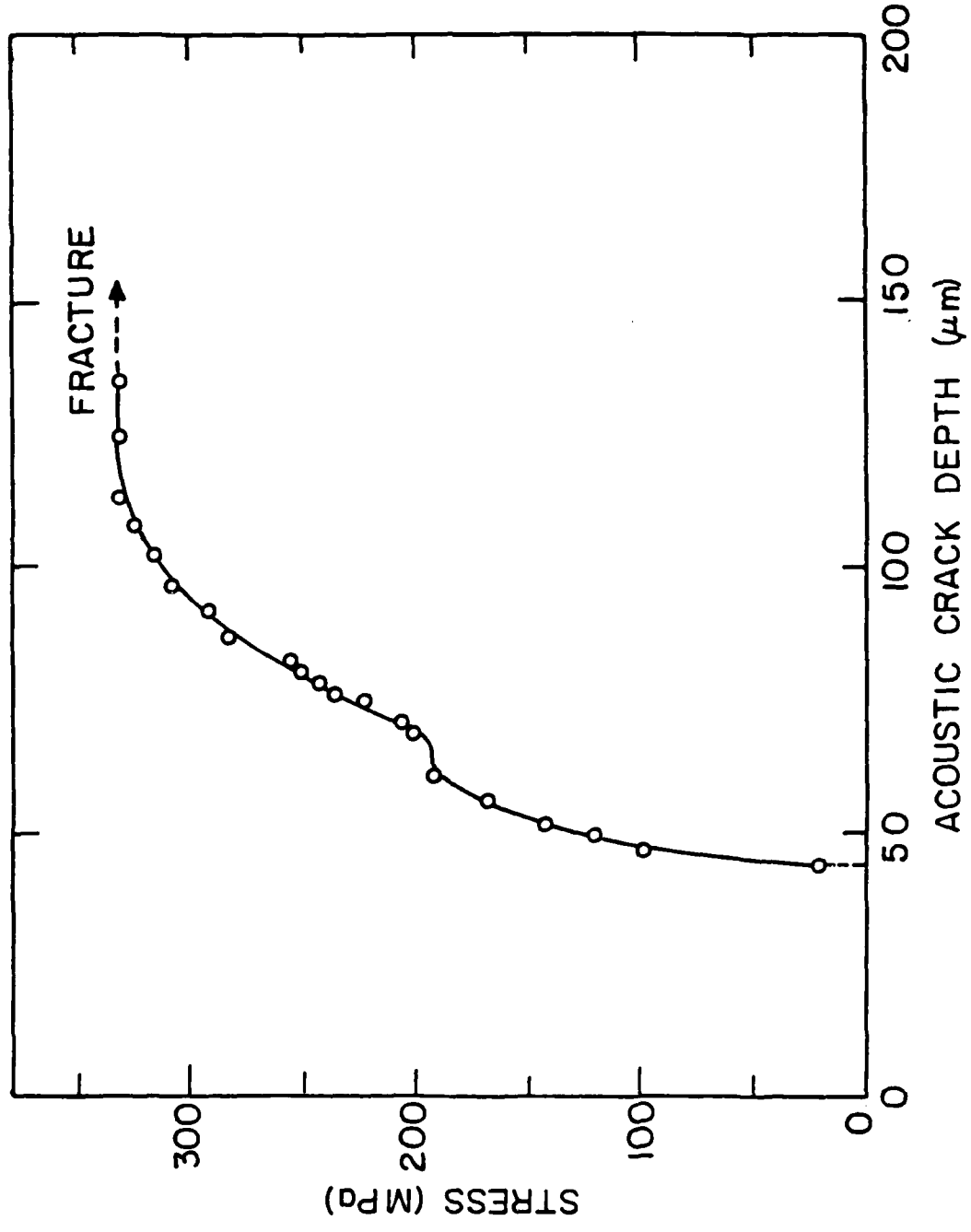




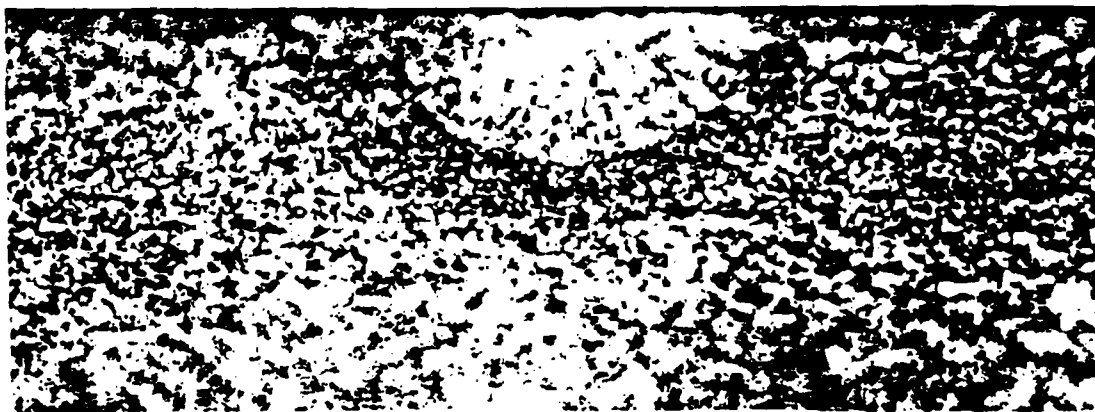
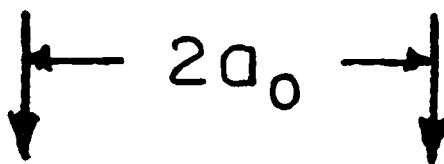
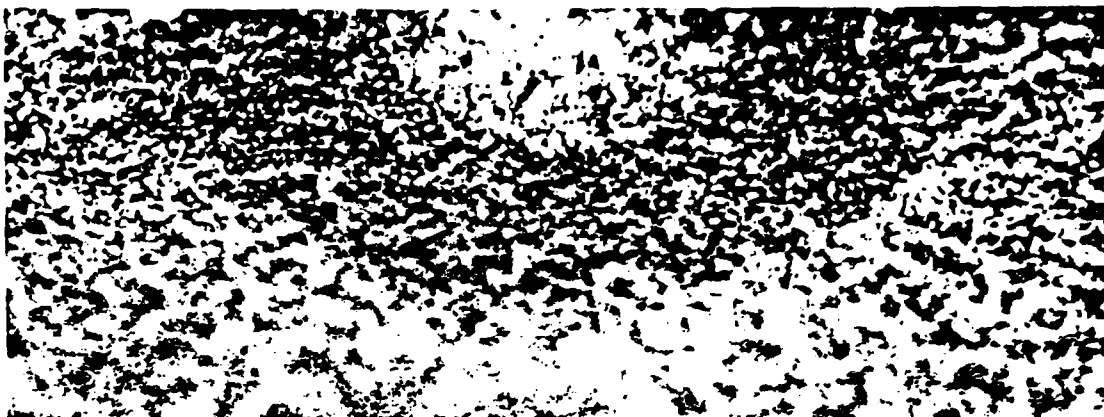
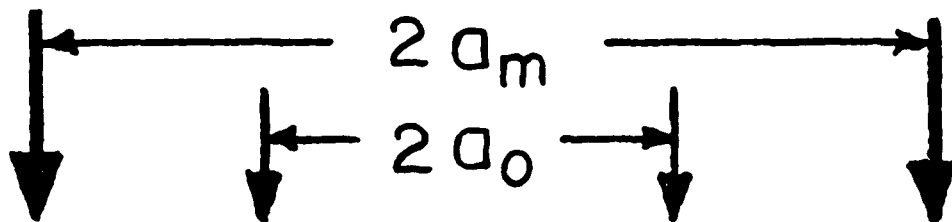
XBL 8012-13376

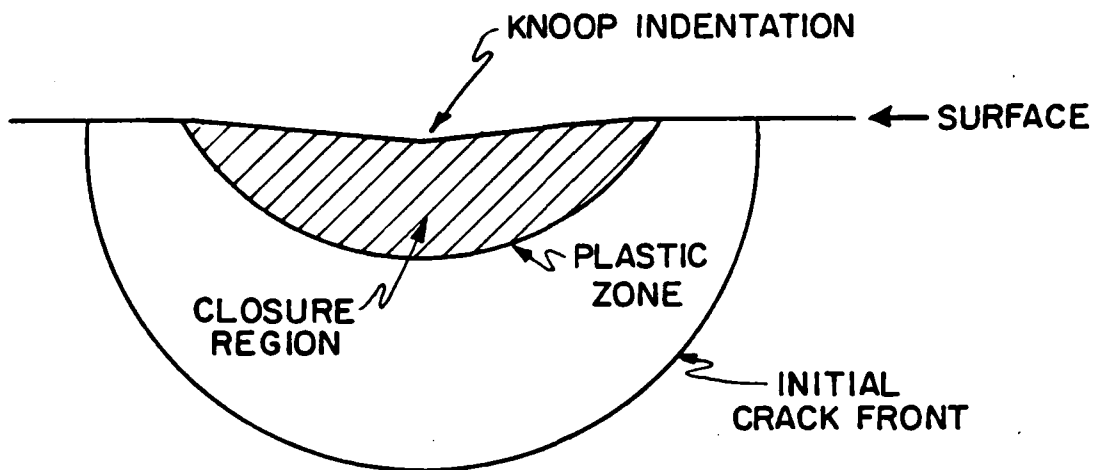


XBL 8012-13377

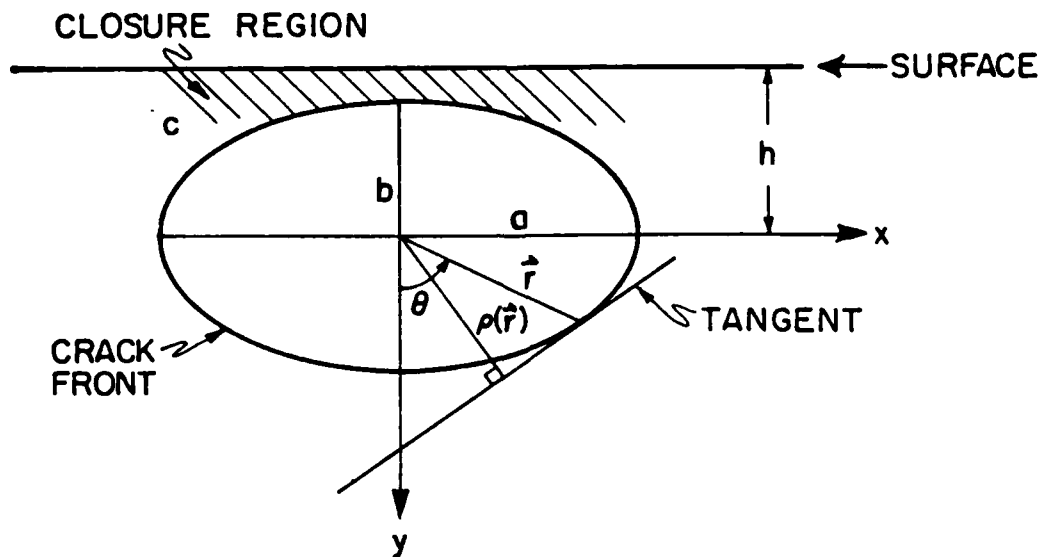


XBL 8012-13378

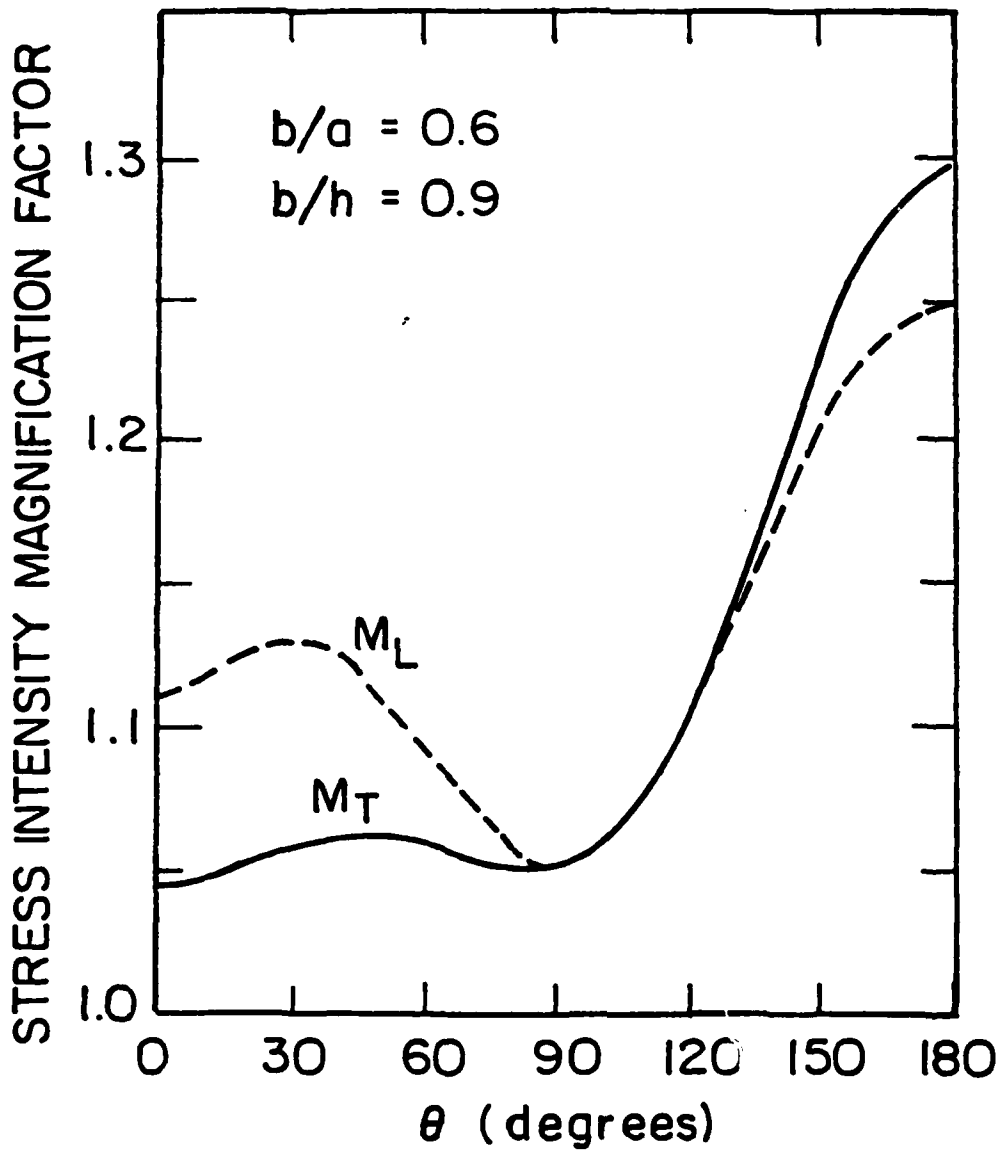




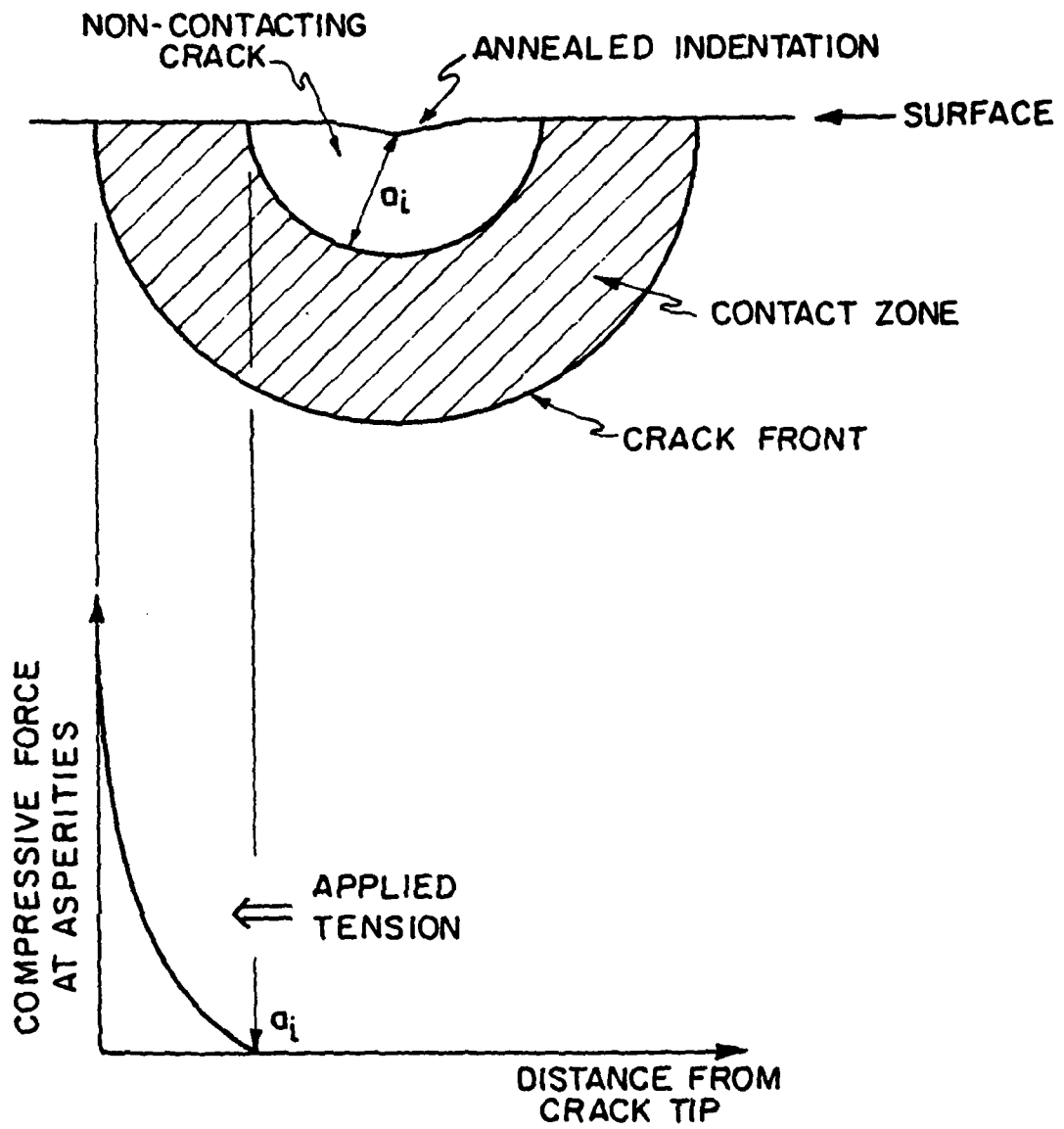
a) AS-INDENTED CRACK CONFIGURATION



b) CRACK MODEL FOR ACOUSTIC SCATTERING ANALYSIS



XBL8012-13380



XBL 8012-13381

## APPENDIX A

### SURFACE ACOUSTIC WAVE MEASUREMENTS OF SURFACE CRACKS IN CERAMICS

J. J. W. Tien, B. T. Khuri-Yakub, and G. S. Kino  
Edward L. Ginzton Laboratory  
Stanford University  
Stanford, California 94305

and

A. G. Evans and D. Marshall  
Materials Sciences  
University of California  
Berkeley, California 94720

#### ABSTRACT

We have extended our earlier investigation of scattering from surface cracks. In particular, we have studied the change in the reflection coefficient of a Rayleigh wave incident on a half-penny shaped surface crack along with the corresponding change in the acoustic crack size estimates as the cracked sample is stressed to fracture. We have examined in this manner both cracks in annealed samples and as-indentured cracks. We have found that the fracture behavior for cracks in these two types of samples differ quite significantly, with the cracks in the annealed samples exhibiting a partial crack closure characteristic and the cracks in the as-indentured samples displaying both crack closure and crack growth effects.

#### INTRODUCTION

This work is an extension of our earlier study<sup>1</sup> aimed at the establishment of procedures for locating and characterizing surface cracks in structural ceramics. The basic technique we have been using consists of launching a Rayleigh wave on the surface of the ceramic and observing the reflections of the acoustic surface wave from the crack. The particular type of crack we have been studying is a half-penny shaped surface crack introduced at a given orientation into the ceramic surface by a Knoop hardness indenter. In a previous paper,<sup>1</sup> we described a scattering theory valid in the low frequency regime based on the model of an open half-penny shaped crack. This theory related the reflection coefficient measured in the experiment with the crack size and fracture stress of the cracked sample. The theory was shown there to give predictions for the fracture stress which were in good agreement with experimental results. However, predictions for the crack size were observed to be considerably less accurate, with crack size estimates for unstressed samples being smaller by factors of two to three than the actual crack sizes measured after fracture.

Since that time we have extended the theory and correlated our results with what would be expected from fracture mechanics studies of ceramics. A series of experiments on annealed and unannealed samples has demonstrated the power of acoustic techniques for studying cracks in ceramics. The work indicates that cracks in annealed samples tend to be in contact over most of their cross-section and open up with applied stress. At the point of fracture, a very slight growth in crack radius is observed. On the other hand, cracks in unannealed as-indentured samples exhibit partial closure at the sample surface. Upon application of stress, crack growth occurs, with crack radii tending to increase on the order of 50%. Upon release of stress, the cracks partially close, with their effective radii decreasing by less than 10%. As stress is further applied, further crack growth

is observed, terminating in fracture at lower applied stresses than for equivalent annealed samples. This hysteresis effect has been observed for the first time acoustically. Both the initial crack radius,  $C_0$ , and final radius,  $C_m$ , can be measured after fracture. The results obtained can be predicted accurately via acoustic techniques and agree well with the predictions of earlier theories and experiments by Marshall.<sup>2,3,4</sup>

An important result of our work is the demonstration that it is highly desirable to anneal ceramics in which surface cracks are likely to be present. Annealing inhibits further crack growth by relieving the residual stresses that are present. As evidence, we note that when unannealed samples are stressed, the crack radius increases by a factor of approximately two. Annealing, however, causes an increase in the fracture stress observed by a factor of approximately 1.5.

#### THEORETICAL REVIEW

A general theory of scattering from flaws developed by Kino and Auld<sup>5,6</sup> forms the basis for our work. The scattering configuration considered is shown in Fig. 1. The reflection coefficient,  $S_{21}$ , is defined as the amplitude ratio of the reflected signal from the flaw,  $A_2$ , received by transducer 2, to the incident signal,  $A_1$ , transmitted by transducer 1, at the terminals of the transducers. In terms of the input power to the transmitting transducer,  $P$ , the Rayleigh wave displacement field when the receiving transducer is used as the transmitter,  $u_j^{(2)}$ , and the applied stress in the vicinity of the flaw before the flaw is introduced,  $\sigma_{ij}^{A(1)}$ ,  $S_{21}$  is given by

$$S_{21} \equiv \frac{A_2}{A_1} = \frac{j\omega}{4P} \int_{S_c} u_j^{(2)} \sigma_{ij}^{A(1)} n_i dS \quad (1)$$

for the case where the flaw is a void. Here, the integral is taken over the entire surface of the void,  $S_c$ .

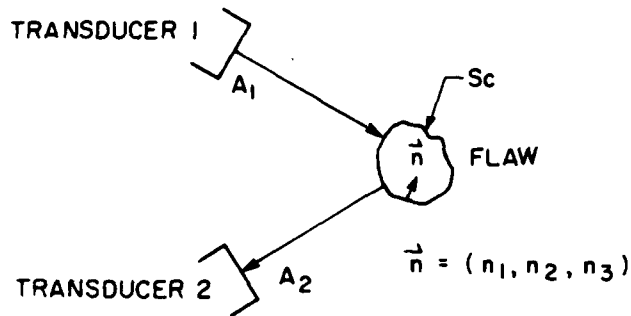


Figure 1 - A schematic of the geometry considered in the derivation of the reflection coefficient,  $S_{21}$ , for a flaw. Here,  $\vec{n}$  is the inward normal to the flaw surface,  $S_c$ .

For the situation of a Rayleigh wave normally incident on a half-penny shaped surface crack of radius  $a$  located in the  $x$ - $y$  plane (Figs. 2 and 3), the reflection coefficient may be written as

$$S_{11} = \frac{j\omega}{4P} \int_S \Delta u_z \sigma_{zz}^A dS \quad (2)$$

where  $\Delta u_z$  is the discontinuity in the Rayleigh wave displacement field across the crack and  $\sigma_{zz}^A$  is the applied stress. The integral is now taken over just the semi-circular area,  $S$ . The theory we have developed for this configuration is strictly valid only in the low frequency regime (i.e. we require the maximum depth to which the crack extends below the sample surface to be much less than an acoustic wavelength). To take into account the effect of imaging at the surface in increasing the value of the stress intensity factor near the surface, as well as the variation with depth of the Rayleigh wave stress fields, we use the results of Budiansky and O'Connell<sup>7</sup> to write the surface integral in Eq. (2) in terms of a contour integral of the square of the mode I stress intensity factor,  $K_I$ , around the crack circumference  $C$  (Fig. 3)

$$\int_S \Delta u_z \sigma_{zz}^A dS = \frac{2(1-\nu^2)}{3E} \int_C a K_I^2(\theta) d\ell \quad (3)$$

Here,  $\nu$  is Poisson's ratio and  $E$  is Young's modulus. The angular dependence of  $K_I$  caused by the surface imaging forces may be approximated from the results of Smith, Emery, and Kobayashi.<sup>8</sup> Smith et al. considered the case of a half-penny shaped surface crack in a beam of thickness  $2c$  subject to a bending load. The applied stress then takes the linear form

$$\sigma_{zz}^A(y) = A(1 - y/c) \quad (4)$$

where  $A$  is a constant and  $y$  is the distance from the sample surface (Fig. 2). The corresponding stress intensity factor is given by

$$K_I(\theta) = 2\sqrt{a/\pi} A[\psi_0(\theta) - (a/c)\psi_1(\theta)] \quad (5)$$

where the functions  $\psi_0(\theta)$  and  $\psi_1(\theta)$  were numerically evaluated by Smith et al. (Fig. 4). To make use of these results for our case where the stress is due to the Rayleigh wave and not a bending load, we made a linear approximation to the Rayleigh wave stress field and so evaluated effective values for the constants  $A$  and  $c$  appearing in Eq. (4). Our result for the normalized reflection coefficient  $wk|S_{11}|$ , for a semi-circular crack, as a function of the normalized crack depth,  $2\pi a/\lambda$ , is given by the dashed curve in Fig. 5. Here  $k = 2\pi/\lambda$  is the propagation constant of the Rayleigh wave, and  $w$  is the width of the acoustic beam at the crack.

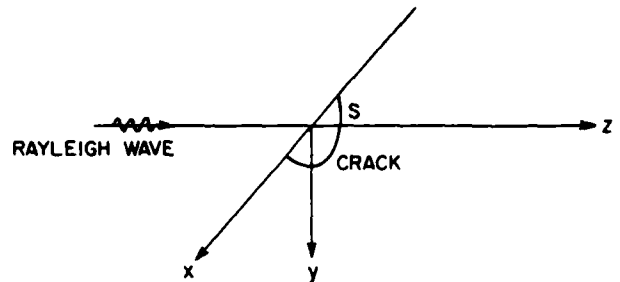
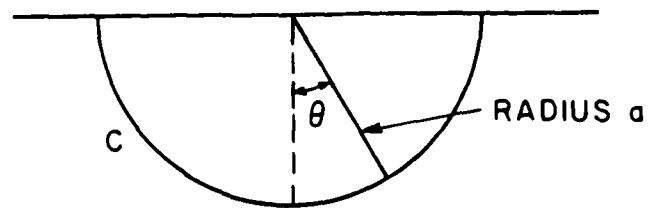


Figure 2 - Scattering geometry for a Rayleigh wave normally incident on a half-penny shaped crack.



### HALF - PENNY SHAPED CRACK

Figure 3 - Schematic of half-penny shaped crack geometry.

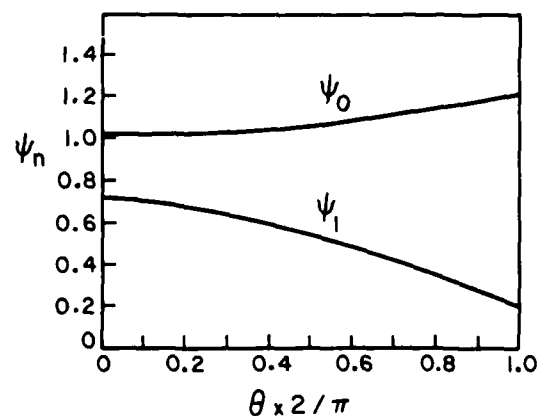


Figure 4 - Angular variation of the functions  $\psi_0(\theta)$  and  $\psi_1(\theta)$  (after Smith et al.<sup>8</sup>).

### EXPERIMENTAL RESULTS

In our experimental studies, we used a commercial hot-pressed silicon nitride (NC-132) ceramic. The samples were in the form of 7.6 cm x 2.6 cm x .64 cm plates with polished surfaces into which cracks had been introduced via a Knoop indenter.

Measurements were made at a frequency of about 8.5 MHz, corresponding to an acoustic wavelength of about 680  $\mu\text{m}$ . Two wedge transducers in the configuration shown in Fig. 6 were used to excite and receive the acoustic signals. The experimental values for the reflection coefficient thus obtained were then corrected for diffraction loss, the surface wave conversion efficiencies of the transducers, and for the effect of the transmitted and reflected acoustic beams each being at an angle  $\alpha$  from the crack normal.

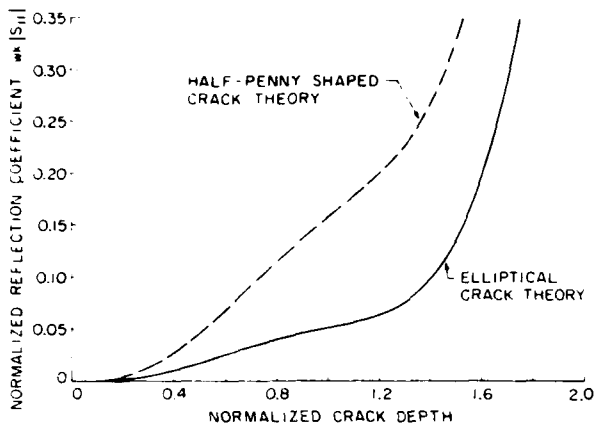


Figure 5 - Comparison of the results for the normalized reflection coefficient,  $wk|S_{11}|$ , as a function of the normalized crack depth for the half-penny shaped crack theory and the elliptical crack theory. The normalized crack depth is defined for each theory by the quantities  $2\pi a/\lambda$  and  $2\pi(b+h)/\lambda$ , respectively.

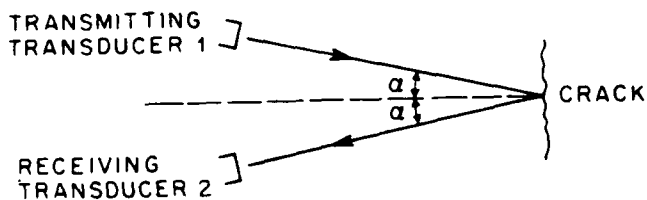


Figure 6 - Experimental scattering configuration used. In our study,  $\alpha = 12.5^\circ$ .

Measurements were carried out on both annealed and as-indented samples. One sample was annealed in air and another in a vacuum with an annealing period of about six hours at a temperature of 1200°C. An additional three samples were tested in their as-indented state. For all five samples, we monitored the change in the acoustic reflection coefficient while the samples were slowly stressed to fracture in a 3-point bending jig.

**Annealed Samples** - We found that the cracks in the annealed samples are fairly well modelled by the open half-penny shaped crack theory described in the previous section, subject to the additional observation that in the unstressed state, partial crack closure occurs (Fig. 7). As shown in Figs. 8 and 9, loading the sample from zero stress to fracture produces a steady increase in the acoustic prediction for the crack depth. We additionally observe that if, after a period of loading, the load is reversed until the stress in the vicinity of the crack approaches zero, the crack size estimates tend to return to very near the initial value

observed for the unstressed sample (Fig. 9). Application of a load to the cracked sample thus has the effect of causing the crack to open, as indicated by the increase in the acoustic size estimates with increasing load; however, subsequent removal of the load results in a return of the crack to its original partially closed state. Verification of this interpretation is obtained upon inspection of the fracture surface (Fig. 10). Here, only the initial flaw produced by the Knoop indenter is in evidence, as indicated by the single ring near the sample surface. Lastly, we compare the acoustic estimate for the crack depth at fracture with the optically measured crack depth (Table I). For both samples, agreement between these two values is quite good, with the deviation of the acoustically predicted values from the actual values being less than 17%.

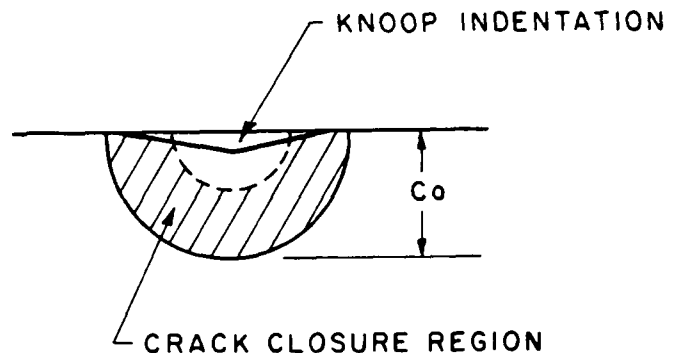


Figure 7 - Fracture model for crack in an annealed sample.  $C_0$  is the depth of the initial flaw produced by the Knoop indenter. In the unstressed state, the crack is partially closed, as indicated.

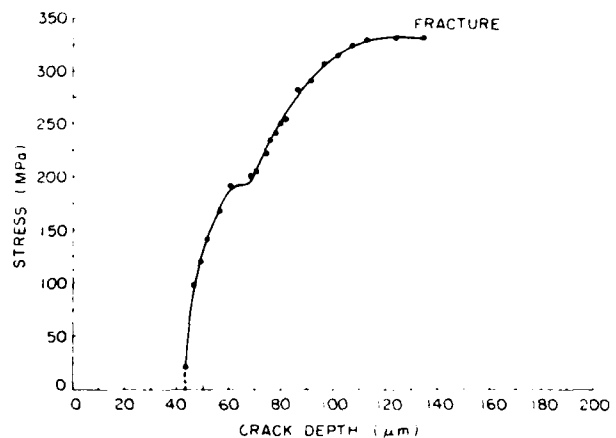


Figure 8 - Stress versus acoustic estimates of the crack depth for the sample annealed in air (sample 1). Crack depth estimates are obtained using the half-penny shaped crack theory (crack depth,  $C$ , then equals the half-penny shaped crack radius,  $a$ ). The kink observed in the curve is believed to be an effect of the severe surface oxidation which occurred during the annealing process.

**As-Indented Samples** - The fracture model for the cracks in the as-indented samples differs considerably from the model for the cracks in the annealed samples. Firstly, there is crack closure at the sample surface in the vicinity of the Knoop indentation (Fig. 11). This arises because the Knoop indentation technique used to produce the crack creates a plastic deformation

region in the neighborhood of the indentation in which the residual stress fields have not been relieved as in the annealed samples. The second difference is that as the cracked sample is stressed to fracture, the crack grows from an initial depth of  $C_0$  to a final fracture depth of  $C_m$ .

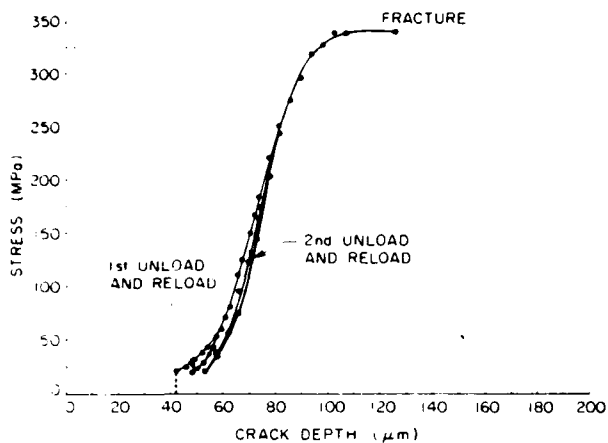


Figure 9 - Stress versus acoustic estimates of the crack depth for the vacuum-annealed sample (sample 2). Two unload-reload cycles were performed on this sample. Crack depth estimates were obtained using the half-penny shaped crack theory (crack depth,  $C$ , equals half-penny shaped crack radius,  $a$ ).



Figure 10 - Typical fracture surface for crack in an annealed sample.

The first problem that we encounter is that our earlier scattering theory based on the model of an open half-penny shaped crack no longer is applicable here. We have not yet developed a theory which accurately models the surface closure characteristic of these as-indented cracks; however, we have worked out a theory based on a very crude approximation for the actual crack configuration which gives surprisingly good crack size predictions. This theory approximates the actual crack

by an elliptical crack with semi-major axis  $a$  and semi-minor axis  $b$  where the surface closure effect is modelled by removing the elliptical crack center to a position a distance  $h$  below the sample surface ( $b < h$ ; Fig. 12). We can evaluate the reflection coefficient for a Rayleigh wave normally incident on this type of crack configuration much as we did earlier. Again, the reflection coefficient is given by Eq. (2). Here, however, we must use a generalized form of Eq. (3) to relate the surface integral in Eq. (2) to the contour integral involving the stress intensity factor,  $K_I$ , namely

$$\int_S \Delta u_z \sigma_{zz}^A dS = \frac{2(1 - \nu^2)}{3E} \int_C \rho(\vec{r}) K_I^2(\theta) d\ell \quad (6)$$

In Eq. (6), the quantity  $\rho(\vec{r})$  is defined for a given point  $\vec{r}$  on the crack circumference  $C$  as the perpendicular to the tangent line at  $\vec{r}$ , which passes through the origin of the crack coordinate system. Shah and Kobayashi<sup>9</sup> have evaluated the angular dependence of the stress intensity factor for this type of crack subject to a bending load. The form for the applied stress is again linear

$$\sigma_{zz}^A(y) = C_1 + C_2 \frac{b - y}{b} \quad (7)$$

where  $C_1$  and  $C_2$  are constants. In terms of  $C_1$  and  $C_2$ , and the functions  $M_T(\theta)$  and  $M_L(\theta)$  numerically evaluated by Shah and Kobayashi, the stress intensity factor may be written in the form

$$K_I(\theta) = \frac{\sqrt{\pi b/a}}{E(k)} (a^2 \cos^2 \theta + b^2 \sin^2 \theta)^{1/4} \left\{ C_1 M_T(\theta) + C_2 M_L(\theta) \left[ 1 - \frac{k^2 E(k) \cos \theta}{(1 + k^2) E(k) - (k')^2 K(k)} \right] \right\} \quad (8)$$

Here,  $K(k)$  and  $E(k)$  are complete elliptic integrals of the first and second kinds, respectively, and the quantities  $k$  and  $k'$  are defined by

$$k^2 = 1 - (b/a)^2$$

$$(k')^2 = (b/a)^2 \quad (9)$$

$M_T(\theta)$  and  $M_L(\theta)$  represent the stress intensity magnification factors for the elliptical crack configuration shown in Fig. 12 for the respective cases of a uniform applied stress and a linearly varying applied stress. These functions have been calculated by Shah and Kobayashi for various values of the aspect ratio,  $b/a$ , and the depth ratio,  $b/h$ . As in the actual crack, the crack width is roughly twice the crack depth, and the region of surface closure is shallow compared to the maximum crack depth. We have chosen to use the Shah and Kobayashi results for  $M_T(\theta)$  and  $M_L(\theta)$  given for the parameter values  $b/a = 0.6$  and  $b/h = 0.9$  (Figs. 13 and 14). The result for the normalized reflection coefficient,  $wk|S_{11}|$ , as a function of the normalized crack depth  $2\pi(b+h)/\lambda$ , is then given by the solid curve in Fig. 5.

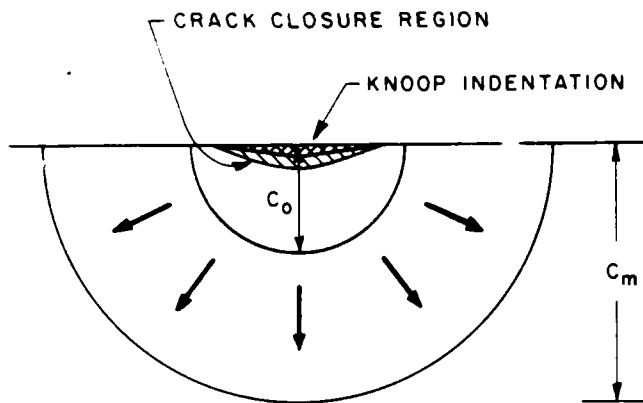


Figure 11 - Fracture model for an as-indented crack.  $C_0$  is the depth of the initial flaw produced by the Knoop indenter;  $C_m$  is the depth to which the crack grows before fracturing. Crack closure occurs at the surface in the vicinity of the Knoop indentation.

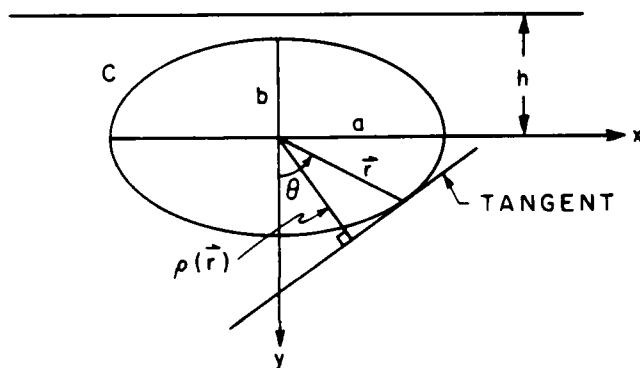


Figure 12 - Schematic of elliptical crack theory geometry.

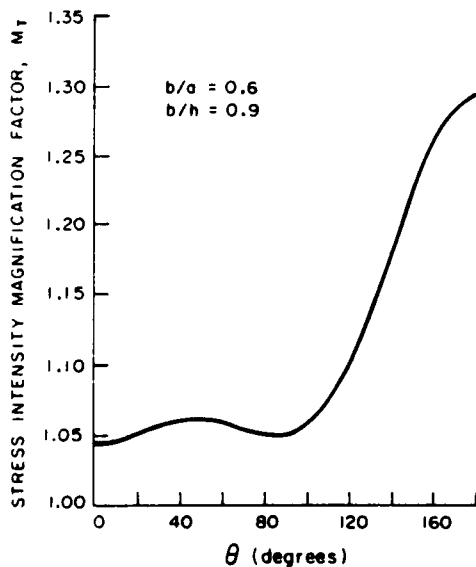


Figure 13 - Stress intensity magnification factor as a function of the angle  $\theta$  for the elliptical crack configuration of Fig. 12, subject to a uniform applied stress (after Shah and Kobayashi<sup>9</sup>).

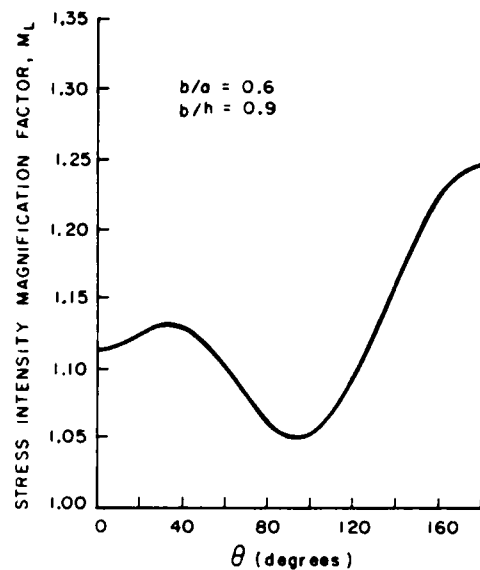


Figure 14 - Stress intensity magnification factor as a function of the angle  $\theta$  for the elliptical crack configuration of Fig. 12, subject to a linearly varying applied stress (after Shah and Kobayashi<sup>9</sup>).

We used this crude theoretical model to give crack size estimates for the as-indented samples. As with the cracks in the annealed samples, there is a steady increase in the crack depth estimates with increasing load (Figs. 15, 16, and 17). However, with these cracks, crack growth occurs, as indicated by the failure of the cracks to return to their original sizes upon subsequent unloading. In addition, a small decrease in the crack size estimates is observed when the load is relieved, thus indicating a slight tendency of the cracks towards partial closure at the lower boundary upon unloading. Continuous growth of the crack until fracture is evidenced in Fig. 16 where two unload-reload cycles were performed. In each cycle, it is apparent that the crack never fully returns to the size it had previously when the stress is reduced to near zero values.

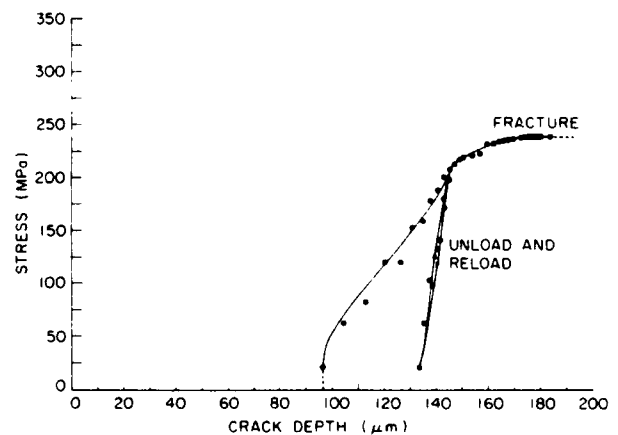


Figure 15 - Stress versus acoustic estimates of the crack depth for as-indented sample 4. One unload-reload cycle was performed. The crack depth,  $C$ , equals the quantity  $b + h$  (see Fig. 12).

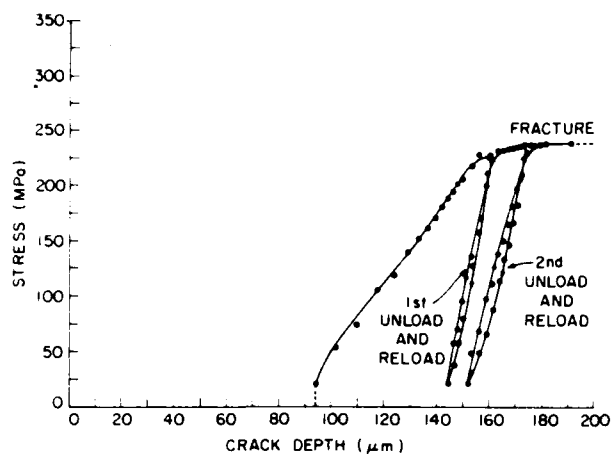


Figure 16 - Stress versus acoustic estimates of the crack depth for as-indented sample 5. Two unload-reload cycles were performed. The crack depth,  $C$ , equals the quantity  $b + h$  (see Fig. 12).

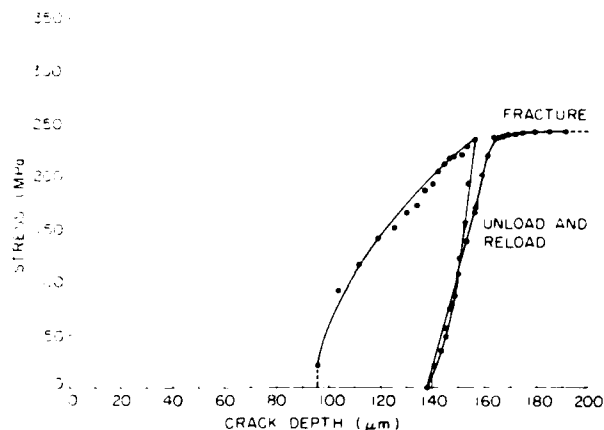


Figure 17 - Stress versus acoustic estimates of the crack depth for as-indented sample 6. One unload-reload cycle, where the sample was fully unloaded, was performed. The crack depth,  $C$ , equals the quantity  $b + h$  (see Fig. 12).

Examination of a typical fracture surface for these samples reveals the presence of two rings near the sample surface (Fig. 18). The inner ring represents the extent of the initial flaw produced at the time of indentation. The outer ring indicates the extent to which the crack grew before fracture occurred. A comparison of the acoustic estimates for the initial crack depth,  $C_0$ , and the depth at fracture,  $C_m$ , with the corresponding values measured optically is given in Table II. Considering the crudeness of the model used to obtain the acoustic estimates, the agreement between these values is remarkably good.

Lastly, we compare the fracture stresses of the five samples. From Tables I and II, we note that the crack depths at fracture for the annealed samples tend to be much less than those for the as-indented samples. Thus, we expect the annealed samples to fracture at higher stress values than the as-indented samples. In Table III, we show that this is indeed the case.



Figure 18 - Typical fracture surface for crack in an as-indented sample.

#### CONCLUSION

We conclude that the acoustic technique is a powerful method for observing fracture of surface cracks in ceramics. Major differences in the fracture behavior of cracks in annealed and unannealed samples have been documented.

It is apparent that there is a need to improve the acoustic scattering formulae and the estimates of the stress intensity factor for cracks closed at the sample surface. A theory by which to accurately predict how a partially closed annealed crack opens under applied stress would also be of considerable interest. We are currently developing a variational method to deal with the problems encountered in the scattering theory and are considering simple theories to deal with the latter problem.

#### Acknowledgement

This work was supported by the Office of Naval Research under Contract No. N00014-78-C-0283.

TABLE I: Annealed Samples

Sample	Acoustic $C_m$ ( $\mu\text{m}$ )	Actual $C_m$ ( $\mu\text{m}$ )	Deviation
1	134	115	17%
2	125	115	7%

TABLE II: As-Indented Samples

$C_0$  = initial crack depth

$C_m$  = crack depth at fracture

$C_0 < C_m$

Sample	Acoustic $C_0$ ( $\mu\text{m}$ )	Actual $C_0$ ( $\mu\text{m}$ )	Deviation
4	97	116	16%
5	94	112	16%
6	96	112	14%

Sample	Acoustic $C_m$ ( $\mu\text{m}$ )	Actual $C_m$ ( $\mu\text{m}$ )	Deviation
4	184	220	16%
5	191	223	14%
6	185-191	205	7-10%

TABLE III: Fracture Stresses

	Sample	Fracture Stress (MPa)
Annealed:	1	332
	2	340
As-Indented:	4	238
	5	239
	6	242

References

- 1: J. Tien, B. Khuri-Yakub, and G.S. Kino, "Acoustic Surface Wave Probing of Ceramics," Proc. ARPA/AFML Rev. of Progress in Quantitative NDE, La Jolla, California, July 1979.
- 2: D.B. Marshall and B.R. Lawn, "Residual Stress Effects in Sharp Contact Cracking: Part 1, Indentation Fracture Mechanics," J. Matls. Science, vol. 14, pp. 2001-2012, 1979.
- 3: D.B. Marshall, B.R. Lawn, and P. Chantikul, "Residual Stress Effects in Sharp Contact Cracking: Part 2, Strength Degradation," J. Matls. Science, vol. 14, pp. 2225-2235, 1979.
- 4: B.R. Lawn and D.B. Marshall, "Residual Stress Effects in Failure From Flaws," J. Am. Ceramic Soc., vol. 62, no. 1-2, pp. 106-108, Jan-Feb 1979.
- 5: G.S. Kino, "The Application of Reciprocity Theory to Scattering of Acoustic Waves by Flaws," J. Appl. Phys., vol. 49, no. 6, pp. 3190-3199, June 1978.
- 6: B.A. Auld, "General Electromechanical Reciprocity Relations Applied to the Calculation of Elastic Wave Scattering Coefficients," Wave Motion, vol. 1, no. 1, pp. 3-10, January 1979.

- 7: B. Budiansky and R.J. O'Connell, "Elastic Moduli of a Cracked Solid," Int. J. Solid Structures, vol. 12, pp. 81-97, Pergamon Press, 1976.
- 8: F.W. Smith, A.F. Emery, and A.S. Kobayashi, "Stress Intensity Factors for Semicircular Cracks: Part 2, Semi-Infinite Solid," J. Appl. Mech., vol. 34, no. 4, pp. 953-959, December 1967.
- 9: R.C. Shah and A.S. Kobayashi, "On the Surface Flaw Problem," The Surface Crack Physical Problems and Computational Solutions, J.L. Swedlow, ed. pp. 79-124; presented at the Winter Annual Meeting of the ASME, New York, New York, November 1972.
- 10: G.S. Kino, "Variational Formulae for Scattering of Acoustic Waves by Flaws and for Acoustic Wave Propagation," Ginzton Laboratory Report No. 2634, Stanford University, November 1976.
- 11: G.S. Kino, "Variational Methods for Calculating J and M Integrals and Acoustic Scattering From Cracks," Materials Research Council Report, July 1980.

MAY 13 1981 *WC REP*

*059-101*

MEASUREMENT OF SURFACE DEFECTS IN CERAMICS

End of Year Report, 1980

Principal Investigator

G. S. Kino  
(415) 497-0205

Associate Investigator:  
B. T. Khuri-Yakub

Consultant:  
A. G. Evans

*Quality  
checked*  
*All  
reports  
checked*

Contract N00014-78-C-0283  
Contract Period: 1 March 1980 - 28 February 1981  
Amount of Contract: \$200,812

Scientific Officer:

Dr. Arthur M. Diness  
Director, Metallurgy and  
Ceramics Program  
Materials Sciences Division  
Office of Naval Research  
Department of the Navy  
800 North Quincy Street  
Arlington, Virginia 22217

G. L. Report No. 3256

April 1981

Edward L. Ginzton Laboratory  
W. W. Hansen Laboratories of Physics  
Stanford University  
Stanford, California

8 1 6 12 076

## MEASUREMENTS OF SURFACE DEFECTS IN CERAMICS

### Introduction

During the past year we have continued our acoustic surface wave measurements of the scattering coefficients of surface cracks in ceramics. The aim is to measure the size of the surface cracks and predict the failure stress of parts containing them.

The research has been extremely successful; we can now make accurate predictions of failure stress of unannealed samples containing penny-shaped cracks in the 100-300  $\mu\text{m}$  range. By changing the frequency, the basic technique should, in fact, be usable over a far greater range in both directions(directions?) of crack sizes. Not only can we predict the failure stress when the applied stress is perpendicular to the direction of the crack, but we can also make predictions accurate to within 20% of the failure stress of cracks at angles up to 45% to the applied stress, provided we make the acoustic wave measurement in the direction of the applied stress.

We have studied the effects of residual stress on crack size estimation, fracture stress and slow crack growth, and now have a very good understanding of the effects of plasticity and residual stress in ceramics. The acoustic measurements have enabled us to watch a crack grow and to examine the effects of crack closure. Thus, they have provided an important new experimental tool for fundamental studies of crack growth in ceramics. We are presently extending our study to evaluate the effects of surface roughness and machine damage on crack size estimation and fracture.

### Research Progress

The acoustic surface wave measurement of the surface cracks is carried out at a frequency of 8 MHz, and the cracks range in size from 50 to 300  $\mu\text{m}$ . Thus, we operate in the region of  $ka = .5$  to  $ka = 3$ . We have already reported on the theory developed to measure the size of surface cracks from a scattering measurement in the low  $ka$  regime. However, our initial theory did not take into account the effect of residual stress on crack sizing and fracture prediction. This deficiency in the theory was evidenced experimentally by undersizing the surface cracks by a factor of 2 or more. At the end of the last reporting period, we realized that due to the residual stress (introduced by the Knoop indenter), the crack tip is closed at the surface, and the reflection coefficient of the crack is greatly reduced. We have now developed a model for such cracks, and can theoretically predict the behavior of surface cracks in the presence or absence of residual stress. We have confirmed this theory experimentally, and can now size cracks and predict the failure of parts containing cracks with an accuracy of less than 20%.

Appendix A is a paper that will be published in the ARPA/AFML Review of Progress in Quantitative NDE, 1980, in which we describe the theory and experimental results on the measurement of surface cracks in silicon nitride. In summary, the Knoop indenter introduces residual stress that closes the crack at its surface. Thus, the crack displacement is reduced, and the reflection coefficient from the crack is reduced as compared to a crack with open crack tips. As a first order approximation, we consider the crack to be elliptical in shape lying just below the surface (10% from total crack depth). We calculate the reflection coefficient of an elliptical embedded

crack, and we use this to predict crack size. Measurements of crack size were made on several samples with and without (annealed) residual stress. We measured the reflection coefficients of the surface cracks as they were stressed to fracture in a three-point bending jig.

Our experiments indicate that annealed samples behave like surface breaking surface cracks, with open-tips (no residual stress), and that no slow crack growth is present, as would be expected in brittle materials. The crack sizes and fracture stresses were predicted with an accuracy of better than 20% (Table I, Appendix A).

In unannealed samples, we found evidence of slow crack growth. Slow crack growth is observed as shown in Figs. 15, 16, and 17 of Appendix A, where the crack does not go back to its initial size when unloading the bending stress in the three-point bending jig. These cracks behaved like buried elliptical cracks just below the surface. The estimate of crack size and fracture stress was again predicted with an accuracy of better than 20%. We have thus a first order model that predicts the behavior and effect of surface cracks when their annealing history is known.

A series of experiments were carried out to measure the reflection coefficients of surface cracks that were oriented at an angle to the long axis of the rectangular test bars. The angle between the long axis of the test bars and the cracks varied from 90 to 45°. The samples were tested with a fixed angle of incidence of the acoustic waves to the long axis of the bars, and, the samples were broken in the same three-point bending jig. No attempt was made to predict the crack size or its growth as the samples were stressed to fracture. Only the reflection coefficient was measured. The crack sizes

were not estimated because the cracks will grow in a direction perpendicular to the direction of the applied stress, thus giving skew-shaped, not planar cracks. The reflection coefficient from the cracks was found on the assumption that an equivalent crack, normal to the direction of incidence of the acoustic wave, existed, and the failure stress was predicted on the basis of the same assumption. The actual fracture stress was predicted with an accuracy of better than 10% for the 10 cracks tested. This result is extremely encouraging. We had indeed expected it because the long wavelength scattering theory we used indicated that the fields of the surface waves are perturbed in the same manner as the field of the static stress applied to fracture.

At the present time, we are carrying out a series of experiments designed to evaluate the effect of machining and surface roughness on the strength of silicon nitride in the presence or absence of surface cracks, and in the presence or absence of residual stress. The samples are being machined and should be tested shortly.

Part of the error in estimating crack sizes from the reflection coefficient measurement is due to the model used for the crack with closed tips (buried ellipse). We have started working on a variational method to predict the reflection coefficient of cracks with odd shapes and mixed boundary conditions (closed or open). Appendix B is a pre-print summarizing the variational technique. So far we have tried the theory on an infinitely long strip crack with a known solution to the crack displacement. By using a trial guess at the displacement, we predict a reflection coefficient that is 10% lower than the exact solution, which results in an error of less than

2% in the value of the stress intensity factor. The variational theory is being programmed so that an optimum computer solution can be generated. We also plan to expand the theory to evaluate the reflection coefficient of two-dimensional cracks of odd shapes.

#### PUBLICATIONS

1. J. Tien, B. T. Khuri-Yakub, G. S. Kino, A. G. Evans, and D. B. Marshall, "Surface Acoustic Wave Measurements of Surface Cracks in Ceramics," Proc. ARPA/AFML Rev. of Progress in Quantitative NDE, La Jolla, California, July, 1980.
2. J. J. W. Tien, B. T. Khuri-Yakub, G. S. Kino, D. B. Marshall, and A. G. Evans, "Surface Acoustic Wave Measurements of Surface Cracks in Ceramics," Submitted to the Journal of Applied Physics, March, 1981.
3. G. S. Kino, "Variational Methods for Calculating J & M Integrals and Acoustic Scattering From Cracks," Proceedings of the MRC Meeting in La Jolla, July, 1980.

#### PRESENTATIONS

1. J. Tien, B. T. Khuri-Yakub, and G. S. Kino, "Surface Crack Evaluation in structural Ceramics," 2nd International Symposium in Ultrasonic Materials Characterization, Gaithersburg, Maryland, June, 1980.

Edward L. Ginzton Laboratory  
W. W. Hansen Laboratories of Physics  
Stanford University  
Stanford, CA 94305  
Contract N00014-78-C-0283

APPENDIX B

VARIATIONAL METHODS FOR CALCULATING J & M  
INTEGRALS AND ACOUSTIC SCATTERING FROM CRACKS

G.S. KINO

ABSTRACT

It is difficult to calculate acoustic scattering coefficients, stress intensity factor and energy integrals of cracks of arbitrary shape and with non uniform applied stress fields. We derive here a variational technique for this purpose, which uses a trial function for the crack opening displacement  $\Delta U$ . We show that the method is easily adaptable to the use of fourier transform techniques and hence can make use of the FFT (fast fourier transform) numerical methods commonly employed in other fields. We give a very simple analytic example of a plane crack in mode I plane strain. Using a crude triangular trial function for the crack opening displacement we obtain interaction energy (M integral) 15% lower than the true value, with a corresponding stress intensity factor 8% lower than the true value. We suggest the use of Rayleigh-Ritz techniques to obtain more accurate results.

81 6 12 070

VARIATIONAL METHODS FOR CALCULATING J & M  
INTEGRALS AND ACOUSTIC SCATTERING FROM CRACKS

G.S. KINO

INTRODUCTION

It is normally difficult to calculate the stress intensity factor of flat crack of arbitrary shape. Similarly, the J & M integrals or the closely related scattering coefficient of an acoustic wave reflected from a crack can only be calculated easily for certain simple crack shapes (ellipses or strips). A further difficult problem is to determine these quantities when the applied stress is non-uniform over the area of the crack.

At the 1975 MRC conference, the author derived an acoustic wave scattering theory <sup>1, 2, 3</sup> which could be stated in variational form. In essence the use of such variational theories could make it possible to employ a trial function  $\Delta U$  for the crack opening displacement. A more accurate guess is then obtained for the energy related quantity of interest such as the M integral or acoustic wave scattering coefficient. The variational method has the advantage of making it possible to use physical intuition in the choice of the trial function and Rayleigh-Ritz techniques to improve the trial function. Furthermore, it lends itself, as we shall see, to the use of FFT (Fast Fourier Transform Techniques) and makes it possible to employ many of the powerful methods that have been used earlier in electromagnetic scattering theories.

Such techniques do not involve the use of singular integral equations nor of Wiener Hopf methods. So, mathematically they are relatively simple and suitable for numerical computation, and are not restricted only to elastostatic solutions. The theory may therefore be useful, ultimately, in applications to acoustic wave scattering theory at arbitrary frequencies.

In this paper we have re-derived the variational theory by a simpler, hopefully, more easily understood method.

We show that it may be generalized to determine not only the scattering coefficient of acoustic waves, but also the interaction energy of a crack and its M integral.

We then go on to demonstrate the use of fourier transform techniques on a simple problem, that of a plane crack in static Mode I plane strain. We show that the use of a relatively crude triangular trial function for the crack opening displacement  $\Delta U = a - |x|$ , instead of the true function  $\Delta U = (a^2 - x^2)^{1/2}$  where  $2a$  is the crack length and  $x$  the distance along its surface, gives an interaction energy and stress intensity factor, 15% and 8% lower than the true values respectively.

## SCATTERING COEFFICIENT AND ENERGY INTEGRALS

We employ the Rayleigh-Betti reciprocity theorem to determine the energy change due to the presence of a flaw. We consider the material to be stressed in a testing machine. Suppose that without a flaw present the displacement, stress and strain at any point in the material are  $U_i^A$ ,  $\sigma_{ij}^A$ , and  $\epsilon_{ij}^A$ , respectively. With the flaw present the displacement and stress at  $U_i$ ,  $\sigma_{ij}$ ,  $\epsilon_{ij}$ , respectively.

By the use of the Rayleigh-Betti reciprocity theorem in the material region outside the flaw, it follows that:

$$\int_S (\sigma_{ij}^A U_j - \sigma_{ij} U_j^A) n_i ds = - \int_{S_F} (\sigma_{ij}^A U_j - \sigma_{ij} U_j^A) n_i ds \quad (1)$$

Where  $S$  is the outer surface of material,  $S_F$  the surface of the flaw, and  $n_i$  the outward normal from these surfaces.

We note that the only contribution to the integral  $S$  comes from the two ends of the material where, we assume it is supported in rigid clamps. ( $\sigma_{ij} n_i = 0$  at a free surface). Then at the clamps  $U_j = U_j^A$ . So it will be seen that the interaction energy with a flaw is  $W$  where:

$$W = \frac{1}{2} \int_S U_j^A (\sigma_{ij}^A - \sigma_{ij}) n_i ds = -\frac{1}{2} \int_{S_F} (\sigma_{ij}^A U_j - \sigma_{ij} U_j^A) n_i ds \quad (2)$$

When the flaw is a crack  $\sigma_{ij} n_i = 0$  on the crack surface. So it follows that the crack energy is

$$W = -\frac{1}{2} \int_{S_F} (\sigma_{ij}^A \Delta U_j) n_i ds \quad (3)$$

Where  $\Delta U_j$  is the crack opening displacement,  $n_i$  is the outward normal on one side of the crack. The energy of a more general flaw is

$$W = \frac{1}{2} \int_{S_F} (\sigma_{ij} U_j^A - \sigma_{ij}^A U_j) n_i ds \quad (4)$$

These results agree with those of Eshelby<sup>4</sup>.

It follows from Budiansky and O'Connell<sup>5</sup> that the interaction energy of a crack is

$$W = \frac{1-\nu^2}{3E} \int_C \rho \left[ K_I^2 + K_{II}^2 + K_{III}^2/(1-\nu) \right] d\ell \quad (5)$$

where  $\rho$  and  $\ell$  are based on the crack based coordinates shown in Fig (1).  $E$  is Young's modulus,  $\nu$  is Poisson's ratio and  $K_I$ ,  $K_{II}$ , and  $K_{III}$  are the stress intensity factors for plane strain and antiplane shear.<sup>5</sup> In turn, Rice's J integral<sup>6</sup> of fracture mechanics is defined as

$$J = \frac{1-\nu^2}{E} \left[ K_I^2 + K_{II}^2 + K_{III}^2/(1-\nu) \right] \quad (6)$$

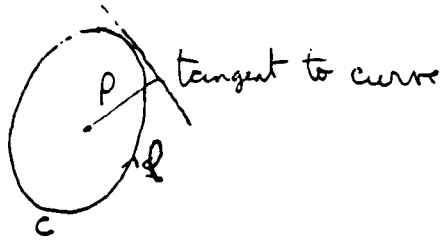


Fig. 1 An illustration of crack based coordinates.

while the M integral of Knowles and Sternberg is defined by the relation

$$M = \int J d\ell \quad (7)$$

It therefore follows that

$$W = M/3 \quad (8)$$

We conclude that if we can evaluate  $W$  we can, in turn evaluate  $M$ . Furthermore, it was shown by Kino that when an acoustic wave is scattered from a crack, the back scatter reflection coefficient of the wave of frequency  $\omega$  is <sup>2,3</sup>

$$S_{11} = \frac{1}{4} j\omega \int_{S_F} (\Delta U_j \sigma_{ij}^A) n_i ds \quad (9)$$

where, now,  $U_j, \sigma_{ij}^A$  are the values of  $U_j, \sigma_{ij}^A$  at the crack when there is unit power emitted by a transducer. So  $S_{11}$  is just  $j\omega W/4$ , with an applied stress equivalent to that of unit power in the incident acoustic wave.

Therefore, if we can evaluate  $W$  correctly, we can determine  $M$  and  $S_{11}$ , parameters of importance in fracture mechanics or in the determination of acoustic wave scattering from a crack. For an exact calculation we need to know the applied field  $\sigma_{ij}^A$  and the crack opening displacement  $\Delta U_j$  in the presence of the applied field. Thus it is necessary to solve for  $\Delta U_j$  when

$$\Delta U_j = 0 \quad \text{outside the crack}$$

$$\sigma_{ij} n_i = 0 \quad \text{at the crack surface}$$

and  $\sigma_{ij}^A$  is known.

## VARIATIONAL THEORY

We have found that the energy stored in a crack is

$$W = \int_S (\sigma_{ij}^A U_j - \sigma_{ij} U_j^A) n_i ds \quad (10)$$

Suppose we use a trial function for the fields within the interior in which  $U_i, \sigma_{ij}$  etc. differ to 1st order error from the correct quantities  $U_i^0, \sigma_{ij}^0$ . Then if we consider the quantity, called the reaction, by Rumsey<sup>8</sup>

$$\Delta W = \int_S (\sigma_{ij} U_j^0 - \sigma_{ij}^0 U_j) n_i ds \quad (11)$$

taken around the outer periphery, we see that when  $\sigma_{ij} = \sigma_{ij}^0$ ,  $U_j = U_j^0$   $\Delta W = 0$ .

Suppose now we require  $\Delta W$  to differ from zero only to 2nd order in error. Then if  $U_j$  is the applied displacement at the grips  $U_j = U_j^0 = U_j^A$ .

So

$$\begin{aligned} \Delta W &= \int (\sigma_{ij} - \sigma_{ij}^0) U_j^A n_i ds \\ &= \int (\sigma_{ij} - \sigma_{ij}^A) U_j^A n_i ds - \int (\sigma_{ij}^A - \sigma_{ij}^0) U_j^A n_i ds \\ \Delta W &= \int (\sigma_{ij} - \sigma_{ij}^A) U_j^A n_i ds - W \end{aligned} \quad (12)$$

It therefore follows that if  $\Delta W = 0$  to 2nd order in error,

$$W = \frac{1}{2} \int (\sigma_{ij} - \sigma_{ij}^A) U_j^A n_i ds \quad (13)$$

is a formula for  $W$ , a correct to 2nd order in error when trial functions  $U_j, \sigma_{ij}$  are employed.

But it follows from the Betti-Rayleigh reciprocity theorem that

$$\Delta W = - \int_{S_F} (\sigma_{ij} U_j^0 - \sigma_{ij}^0 U_j) n_i ds \quad (14)$$

at the flaw.

If the flaw is a crack  $\sigma_{ij}^0 n_i = 0$  at the crack surface and so  $\Delta W$  becomes

$$\Delta W = - \int_{S_F} (\Delta U_j^0 \sigma_{ij}) n_i ds = 0 \quad (15)$$

is the requirement for zero 1st order error in  $W$ , where  $n_i$  is the outward normal from one surface of the crack. But  $\sigma_{ij} n_i$  is only non zero at the crack to 1st order in error. Hence we can replace  $\Delta U_j^0$  by  $\Delta U_j$  and only contribute terms in error to 2nd order in  $\Delta W$ . So

$$\Delta W = - \int_{S_F} (\Delta U_j \sigma_{ij}) n_i ds = 0 \quad (16)$$

is an equally valid assumption.

It follows that Eq. (16) is the requirement for our variational principle. It requires continuity of

$$\int (\sigma_{ij} \Delta U_j) n_i ds$$

through the crack instead of the far more stringent boundary condition:  $\sigma_{ij} n_i = 0$ .

Now consider  $W$ . When we use a trial function  $\Delta U_i$ , it follows that

$$W = \frac{1}{2} \int \left[ (\sigma_{ij} - \sigma_{ij}^S) \Delta U_j \right] n_i ds \quad (17)$$

Where the total field is

$$\sigma_{ij} = \sigma_{ij}^A + \sigma_{ij}^S \quad (18)$$

So  $\sigma_{ij}^S$  is the stress field due to the displacement  $\Delta U_i$ . Because

$$\int (\sigma_{ij} \Delta U_j) n_i ds = 0$$

we see that

$$W = \frac{1}{2} \int (-\sigma_{ij}^S \Delta U_j) n_i ds \quad (19)$$

But as we do not know the amplitude  $\Delta U_j$  and  $\sigma_{ij}^S$  is proportional to  $\Delta U_j$ , we could equally well replace  $\Delta U_j$  by  $A \Delta U_j$ , where  $A$  is a proportionality factor. In this case it follows that

$$W = -\frac{A^2}{2} \int (\sigma_{ij}^S \Delta U_j) n_i ds \quad (20)$$

However we could equally well have written

$$\sigma_{ij}^A = \sigma_{ij}^0 - \sigma_{ij}^{S0} \quad (21)$$

In this case

$$W = -\frac{A}{2} \int (\sigma_{ij}^{S0} \Delta U_j) n_i ds \quad (22)$$

It follows that as Eqs. (20) and (22) must be identical to 2nd order hence

$$A = \frac{\int (\sigma_{ij}^{SO} \Delta U_j) n_i ds}{\int (\sigma_{ij}^{SO} \Delta U_j) n_i ds} \quad (23)$$

and

$$W = \frac{- \left[ \int (\sigma_{ij}^{SO} \Delta U_j) n_i ds \right]^2}{2 \int (\sigma_{ij}^S \Delta U_j) n_i ds} \quad (24)$$

or

$$W = - \frac{\left[ \int (\sigma_{ij}^A \Delta U_j) n_i ds \right]^2}{2 \int (\sigma_{ij}^S \Delta U_j) n_i ds} \quad (25)$$

This is the variational formula required.

We can prove that this formula is variational by writing

$$\sigma_{ij}^S(\underline{x}) n_i = \int G_{ij}(\underline{x}, \underline{x}') \Delta U_j(\underline{x}') n_i ds' \quad (26)$$

where  $\underline{x}$ ,  $\underline{x}'$  are coordinates on the crack surface, and the Green's function  $G_{ij}(\underline{x}, \underline{x}')$  is normally symmetric in the  $\underline{x}$  and  $\underline{x}'$  coordinates.

It follows from Eqs. (25) and (26) that

$$\begin{aligned} 2\delta W \left[ \int (\sigma_{ij}^{SO} \Delta U_j^0) n_i ds \right] &= 2 \left[ \int (\sigma_{ij}^A \Delta U_j^0) n_i ds \right] \left[ \int (\sigma_{ij}^A \delta(\Delta U_j)) n_i ds \right] \\ &\quad - 4W^0 \int \delta(\Delta U_i) G_{ij}(\underline{x}, \underline{x}') \Delta U_j^0(\underline{x}') n_i ds ds' \end{aligned} \quad (27)$$

Substitution from Eqs. (21) and (26) in Eq. (27) leads to the result  $\delta W = 0$ . So the formula of Eq. (25) is variation.

The theory can be generalized fairly easily using the methods of reference 1 to show that the variational formula for scattering from a crack by a signal incident from transducer 1 and received on transducer 2 is

$$S_{21} = \frac{-j\omega}{4} \frac{\int (\sigma_{ij}^A(1) \Delta U_j^{(2)}) n_i ds \int (\sigma_{ij}^A(2) \Delta U_j^{(1)}) n_i ds}{\int (\sigma_{ij}^S(2) \Delta U_j^{(1)}) n_i ds} \quad (28)$$

Where the supercripts (1) and (2) refer to the fields associated with incident waves from transducers 1 and 2, respectively.

#### FOURIER ANALYSIS AND VARIATIONAL TECHNIQUES FOR A CRACK

The variational methods lend themselves well to the use of Fourier analysis techniques, and in particular the application of the Fast Fourier transform numerical computer routines which are now widely available.

Our basic approach will be to use a trial function for  $\Delta U_z$  on the crack surface  $z = 0$ . Then on the plane  $z = 0$  we can write

$$\Delta U_z(x, y, 0) = \int_{-\infty}^{\infty} \int_{-\infty}^{\infty} \Delta U(\alpha, \beta) e^{-j(\alpha x + \beta y)} d\alpha d\beta \quad (29)$$

with

$$\Delta U_z(\alpha, \beta) = \frac{1}{4\pi^2} \int \Delta U_z e^{-j(\alpha x + \beta y)} dx dy \quad (30)$$

It is relatively easy to write down the Fourier transform of other quantities  $U_x, U_y, U_z, \sigma_{zz}, \sigma_{xx}, \sigma_{xy}$ . Then at any point

in space we can use the plane wave angular spectrum analysis to find the connections between these various quantities.

If for instance,  $\sigma_{zz}^S(x,y,0)$  has the Fourier transform  $\sigma_{zz}(\alpha,\beta)$ , it follows from Rayleigh's theorem that

$$\int \sigma_{zz}^S \Delta U_z dx dy = \int \sigma_{zz}(\alpha,\beta) \Delta U^*(\alpha,\beta) d\alpha d\beta \quad (31)$$

Thus it is easy to evaluate the terms we need in the variational theory by relatively simple integrations, and to treat flat cracks of arbitrary shape.

We shall use as an illustration of the variational technique derived here an example calculated for scattering in unpublished work by Kino and Tien, using the earlier 1975 formulation of the variational theory. We take the crack to be located in the  $z=0$  plane, to be of length  $2a$  in the direction and infinitely long in the  $y$  direction, as illustrated in Fig. 2.

We shall treat only the static case of a ~~plane~~ crack with mode I excitation. It will be clear from the treatment how to deal with more complicated situations with time varying excitations and more complicated shapes. We shall compare our results, using simple trial functions, with the exact solution.

We write the displacement in the form

$$\underline{U} = \nabla \phi + \nabla \cdot \underline{\psi} \quad (32)$$

where

$$\nabla^2 \phi + k_\ell^2 \phi = 0 \quad (33)$$

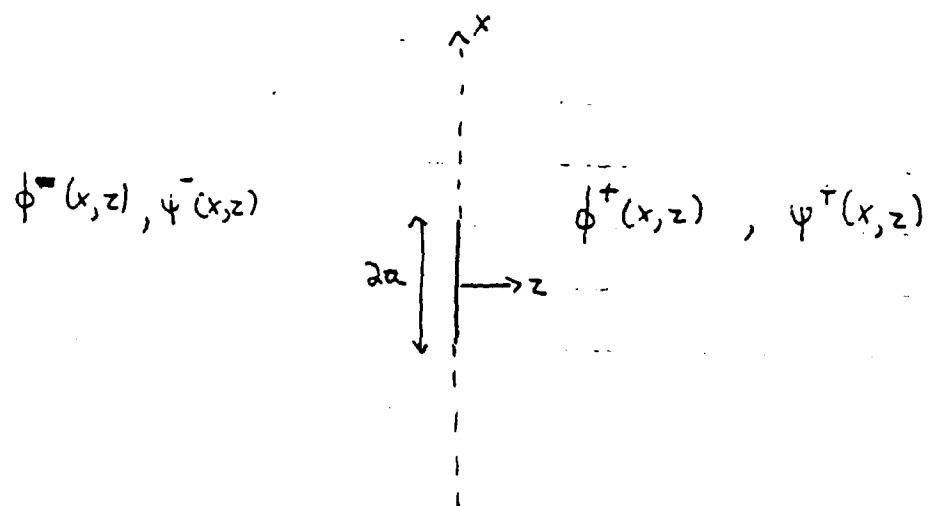


Fig. 2 An illustration of the plane crack used in the theory.

$$\nabla^2 \psi + k_s^2 \psi = 0 \quad (34)$$

with

$$k_l^2 = \omega^2 \rho_{mo} / (\lambda + 2\mu) \quad (35)$$

$$k_s^2 = \omega^2 \rho_{mo} / \mu \quad (36)$$

for waves whose components vary as  $\exp j\omega t$ . The mass density of the material is  $\rho_{mo}$  and the Lamé constants  $\lambda$  and  $\mu$ .

The potentials on each side of the crack are taken to be  $\phi^+(x, z)$ ;  $\psi^+(x, y)$ ; and  $\phi^-(x, z)$ ,  $\psi^-(x, z)$ , respectively.

We can carry out Fourier transforms in the  $x$  direction of these quantities and write

$$\phi^+(x, z) = \int A(\alpha) e^{-j\alpha x} e^{-j\beta_l z} d\alpha \quad (35)$$

$$\psi^+(x, z) = \int B(\alpha) e^{-j\alpha x} e^{-j\beta_s z} d\alpha \quad (36)$$

$$\phi^-(x, z) = \int C(\alpha) e^{-j\alpha x} e^{j\beta_l z} d\alpha \quad (37)$$

$$\psi^-(x, z) = \int D(\alpha) e^{-j\alpha x} e^{j\beta_s z} d\alpha \quad (38)$$

where

$$\alpha^2 + \beta_l^2 = k_l^2 \quad (39)$$

$$\alpha^2 + \beta_s^2 = k_s^2 \quad (40)$$

It will be seen that

$$A(\alpha) = \frac{1}{2\pi} \int \phi^+(x,0) e^{j\alpha x} dx \quad (41)$$

$$B(\alpha) = \frac{1}{2\pi} \int \psi^+(x,0) e^{j\alpha x} dx \quad (42)$$

$$C(\alpha) = \frac{1}{2\pi} \int \phi^-(x,0) e^{j\alpha x} dx \quad (43)$$

$$D(\alpha) = \frac{1}{2\pi} \int \psi^-(x,0) e^{j\alpha x} dx \quad (44)$$

In order to find  $\sigma_{ij}^S$ , we take the boundary conditions at the crack to be

$$\Delta U_z = U_z^+(x,0) - U_z^-(x,0) \quad (45)$$

$$\Delta U_x = U_x^+(x,0) - U_x^-(x,0) = 0 \quad (46)$$

$$\sigma_{zz}^+(x,0) = \sigma_{zz}^-(x,0) = \sigma_{zz}^S \quad (47)$$

$$\sigma_{xz}^+(x,0) = \sigma_{xz}^-(x,0) \quad (48)$$

The use of Eq. (45) with Eqs. (41), (42), and (32) yields the result

$$\beta_L(A + C) + \alpha(B - D) = \frac{j}{2\pi} \int \Delta U_z e^{j\alpha x} dx \quad (49)$$

Similarly from Eq. (46) it follows that

$$\alpha(A - C) - \beta_s(B + D) = 0 \quad (50)$$

It may similarly be shown from Eq. (48) that

$$2\alpha\beta_l(A + C) + (\alpha^2 - \beta_s^2)(B - D) = 0 \quad (51)$$

Where we have used the relation

$$\frac{\lambda + 2\mu}{\mu} = \frac{k_s^2}{k_l^2} = \frac{\alpha^2 + \beta_s^2}{\alpha^2 + \beta_l^2} \quad (52)$$

Continuity of  $\sigma_{zz}$  [Eq. (47)] yields the result

$$(\beta_s^2 - \alpha^2)(A - C) + 2\alpha\beta_s(B + D) = 0 \quad (53)$$

It follows from Eqs. (50) and (53) that

$$A = C \quad (54)$$

$$D = -B \quad (55)$$

So from Eqs. (51), (54) and (55) we see that

$$B = -\frac{2\alpha\beta_l}{\alpha^2 - \beta_s^2} A \quad (56)$$

It therefore follows, after substitution of Eqs. (54), (55) and (56) in Eq. (49) that

$$A = \frac{j}{4\pi} \frac{\beta_s^2 - \alpha^2}{\beta_\ell (\beta_s^2 + \alpha^2)} \int \Delta U_z e^{j\alpha x} dx \quad (57)$$

with

$$\Delta U_z = -2j \int \beta_\ell \frac{\beta_s^2 - \alpha^2}{\beta_s^2 - \alpha^2} A e^{-j\alpha x} d\alpha \quad (58)$$

$$\text{and } \sigma_{zz}^s = -\mu \int A \left[ \frac{(\beta_s^2 - \alpha^2) + 4\alpha^2 \beta_s \beta_\ell}{\beta_s^2 - \alpha^2} \right] e^{-j\alpha x} d\alpha \quad (59)$$

It follows that

$$\int \sigma_{zz}^s \Delta U_z dx = +2j\mu \int_{-\infty}^{\infty} |A|^2 \beta_\ell^2 \frac{(\beta_s^2 + \alpha^2) \left[ (\beta_s^2 - \alpha^2)^2 + 4\alpha^2 \beta_s \beta_\ell \right]}{(\beta_s^2 - \alpha^2)^2} d\alpha \quad (60)$$

We note that  $\beta_s$  and  $\beta_\ell$  must always be positive, i.e. we take their magnitude. So it is convenient to write

$$\int \sigma_{zz}^s \Delta U_z dx = 4j\mu \int_0^{\infty} |A|^2 \frac{(\beta_s^2 + \alpha^2) \left[ (\beta_s^2 - \alpha^2) + 4\alpha^2 \beta_s \beta_\ell \right]}{(\beta_s^2 - \alpha^2)^2} d\alpha \quad (61)$$

If  $A(\alpha)$  is known, this integral can be evaluated numerically.

We put

$$A(\alpha) = R(\alpha) \frac{\beta_s^2 - \alpha^2}{\beta_\ell (\beta_s^2 + \alpha^2)} \quad (62)$$

Where

$$R = \frac{j}{4\pi} \int \Delta U_z e^{j\alpha x} dx \quad (63)$$

So it follows that

$$\int \sigma_{zz}^S \Delta U_z dx = 8j\mu\pi \int_0^{\infty} |R|^2 \frac{[(\beta_s^2 - \alpha^2)^2 + 4\alpha^2 \beta_s \beta_l]}{\beta_l (\beta_s^2 + \alpha^2)} d\alpha \quad (64)$$

We shall now evaluate the static case for which  $k_s \rightarrow 0$ ,  $k_l \rightarrow 0$ . In this case the integral reduces to the form

$$\int \sigma_{zz}^S \Delta U_z dx = -16\mu\pi \int_0^{\infty} |R|^2 \alpha \left( 1 - \frac{k_l^2}{k_s^2} \right) d\alpha \quad (65)$$

or

$$\int \sigma_{zz}^S \Delta U_z dx = -\frac{4E\pi}{(1-\nu^2)} \int_0^{\infty} |R|^2 \alpha d\alpha \quad (66)$$

where  $E$  is Young's modulus,  $\nu$  is Poisson's ratio.

Thus it follows that

$$W = \frac{\left[ \int \sigma_{zz}^A \Delta U_z ds \right]^2}{\frac{8E\pi}{1-\nu^2} \int |R|^2 \alpha d\alpha} \quad (67)$$

Where  $R$  is given by Eq. (63).

We now use the variational formula of Eq. (67) to evaluate

$W$ . We assume  $\sigma_{zz}^A = \text{constant}$ , initially.

Example I: Exact Solution

$$\Delta U_z = K(a^2 - x^2)^{1/2} \quad x < a \quad (68)$$

$$\Delta U_z = 0 \quad x > a$$

In this case it can be shown that

$$R = jK(a/4\alpha) J_1(\alpha a) \quad (69)$$

Where  $J_1(x)$  is a 1st order Bessel function of the 1st kind.

So it follows that

$$W = \frac{8(\sigma_{zz}^A)^2(1-\nu^2)}{\pi E} \frac{\left[ \int_0^a (a^2 - x^2)^{1/2} dx \right]^2}{\int_0^\infty \frac{a^2}{\alpha} J_1^2(\alpha a) d\alpha} \quad (70)$$

This expression yields the correct result:

$$W = \pi a^2 (\sigma_{zz}^A)^2 (1-\nu^2) / E \quad (71)$$

We note, however, that the result obtained is independent of the proportionately factor K.

Now suppose we try the approximate trial function

$$\Delta U_z = K(a - |x|) \quad |x| < a \quad (72)$$

$$\Delta U_z = 0 \quad |x| > a$$

In this case Eq. (67) yields the result

$$W = 2.67a^2 (\sigma_{zz}^A)^2 (1-\nu^2) / E$$

or

$$W_{\text{trial}} / W_{\text{correct}} = 0.85$$

This is a fairly crude result, however, the trial function is also a fairly crude one relative to the correct choice. But with this choice,  $\Delta U$  has dropped to half its maximum value at  $x = 0.5$ , while the true function has dropped to half its maximum value at  $x = 0.87$ . So the stored energy should be higher for the true value of  $\Delta U$ .

#### CONCLUSION

We have derived a variational principle to determine the value of the stored energy or acoustic scattering coefficient of a plane crack. We use the crack opening displacement as a trial function. A simple example for a plane crack using a triangular trial function for  $\Delta U_z$  gave a result with an error of 15%. This would lead to an error of 8% in estimating  $K_I$ . The use of Rayleigh Ritz techniques or a better choice of trial function could improve this result.

The technique is very easy to modify to take account of non-uniform applied stresses. As an example, if we take a bending stress of the form  $\sigma_{zz}^A = \sigma^B |x/a|$ ,  $\Delta U = (a^2 - x^2)^{1/2}$ , we find that

$$W = 0.18\pi a^2 (\sigma^B)^2 (1-\nu^2) / E$$

This would imply that the stress intensity factor is reduced by 0.42 from the value with a uniform applied stress  $\sigma^B$ . The result for the exact solution is a reduction 0.5, so the error is 16%.<sup>9</sup>

Again the use of Rayleigh Ritz methods would be helpful in obtaining more exact results.

#### Acknowledgment

This work was supported by DARPA under Contract MDA 903-76C-0250 with the University of Michigan and by the Office of Naval Research under Contract N00014-78C-0283.

## REFERENCES

1. G. S. Kino, Variational Formulae for Scattering of Acoustic Waves by Flaws, and for Acoustic Wave Profugation, Materials Research Council 1975 Report, also GLG Report # 2634, Ginzton Laboratory, Stanford University, November 1976.
2. G. S. Kino, Perturbation Theory for Scattering of Acoustic Waves by Flaws, Materials Research Council 1975 Report.
3. G. S. Kino, Journal of Applied Physics, 49, 6, 1978.
4. J. D. Eshelby, The Determination of the Elastic Field of an Ellipsoidal Inclusion, and Related Problems, Proc. Roy. Soc. London A 24 1, 376 (1957).
5. B. Budiansky and R. J. O'Connell, Elastic Moduli of a Cracked Solid, Int. J. Solid Structures, 12, 81-97 (1976).
6. J. R. Rice, A Path Independent Integral and the Approximate Analysis of Strain Concentration by Notches and Cracks, J. Appl. Mech (June 1967).
7. J. K. Knowles and E. Sternberg, On a Class of Conservation Laws in Linearized and Finite Elastostatics, Archiv. Rat. Mech. Anal., 44, 3, (1972).
8. J. H. Rumsey, The Reaction Concept in Electromagnetic Theory, Phys. Rev., Ser. 2, 94, 6, 1483-1491, (1954).
9. A. H. Lackenbrush, Depth and Spacing of Tension Cracks, J. Geophysical Research, 66, 12, 4273 - 4292, (1961).

